Rainfall induced instabilities: a field experiment on a silty sand slope in northern Switzerland

Amin Askarinejad,* Francesca Casini,* Patrick Bischof,* Alexander Beck,* Sarah M. Springman*

Abstract

Two full scale field tests were planned and performed successfully on a steep forested slope located on the east facing banks of river Rhine in Ruedlingen, in canton Schaffhausen, northern Switzerland. The aim of the experiments was to study the triggering mechanisms of the landslides due to rainfall. Intensive field investigations were carried out, including in-situ geotechnical tests, characterisation of hydrological properties of the soil and reinforcing effects of vegetation, geological and hydrogeological mapping, and subsurface investigations by means of geophysical methods. Additionally, several series of saturated and unsaturated laboratory tests were conducted on undisturbed and disturbed samples taken from different depths from the vicinity of the selected slope. The test site was intensively instrumented and monitored over a period of 6 months in the course of artificial rainfall and natural precipitation. The instrumentation includes conventional and novel methods to measure pore water pressure, volumetric water content, piezometric height, soil pressure, acoustic emissions, surface and subsurface movements, soil temperature, and meteorological data. This paper introduces briefly the measurements and findings from this multi-disciplinary project, and focuses on numerical and analytical methods used to explain the behaviour of a marginally stable slope before and during the failure induced by rainfall. Simple stability calculations are described that still offer realistic predictions of the status of a slope prone to failure due to increase of the pore water pressure. The basal and lateral reinforcing effects of vegetation and unsaturated shear strength of soil are introduced in these two and three dimensional simulations as well.

1. Introduction

Steep mountainous areas are increasingly endangered by natural hazards. Rainfall induced landslides are one of the major causes of these raised risks. Accordingly, a deeper understanding of the triggering mechanisms of such landslides, and the provision of tools to predict the locations and potential volumes released, is important.

Numerous studies have been conducted to measure the changes in pore water pressure of slopes in response to seasonal and extreme rainfall events. However, few data are available on the hydro-mechanical behaviour of natural slopes during the failure. Ochiai *et al.* [2004] summarised four such experiments. Three of them have been conducted in Japan [Oka, 1972; Yagi *et al.,* 1985; Yamaguchi *et al.*, 1989] and one series of tests was performed by Harp *et al.* [1990] in USA. Ochiai *et al.* [2004] also triggered a fluidised landslide by means of artificial rainfall. Teysseire [2005] mobilised a landslide in the forefield of the Gruben glacier (Canton Wallis, Switzerland).

Harp *et al.* [1990] performed three tests on natural slopes to study the response of the slope to artificial subsurface irrigation in terms of pore water pressure during failure. They induced failure by irrigating the ground artificially through water supply from trenches at the top of the slope and by digging a lower vertical cut, because they had unsuccessful attempts to trigger slope failures by sprinkling with intensities and durations "many times" higher than those of the normal rainfalls. They instrumented the slopes with piezometers and extensometers. The soil types of each site are summarised in table I.

They observed from the lower vertical cut that the water flows, mainly through macropores, during their experiments (e.g. animal burrows and root casts). However, the flow rates from different pores were not constant during the course of irrigation. The authors reported temporal and spatial change of discharge throughout. Harp *et al.* [1990] also measured abrupt decreases in the pore water pressure at different locations of the slopes between 5 to 50 minutes prior to failure. They mentioned simultaneous widening and increase of flow of "muddy water" out of fractures some seconds before failure. They suggest that the raised pore water pressure and increased flow might result in redistribution and removal of fine particles (piping), which may ultimately lead to increase of the pore sizes and destruction of the soil structure at the shear surface. They conclude that loss of contact points between the coarser grains can decrease the shear strength of the material and trigger a landslide.

Ochiai *et al.* [2004] isolated a 5 m wide and 30 m long experimental slope with an average gradi-

* Institute for Geotechnical Engineering, Swiss Federal Institute of Technology, ETH Zurich.

Tab. I – Landslide triggering experiments on natural slopes [modified after OCHIAI *et al.* 2004].
Tab. I – Frane superficiali su pendii naturali [modificata dopo OCHIAI et al. 2004].
* The value is deduced based on the contours on the plan view.

Reference	Location	Triggered Volume or sprinkled area (m^3/m^2)	water supply method	Instrumentation	Slope angle (°)	Soil type
OKA 1972	Japan	500 m^3	Sprayed from fire hose		-	-
YAGI *et al.* 1985	Japan	10 X 25 m^2	Rainfall simulator	Extensometer/Piezometer/ Strain meter	-	-
YAMAGUCHI *et al.* 1989	Japan	10 X 30 m^2	Upper trench	Extensometer/Piezometer/ Inclinometer	-	-
HARP *et al.* 1990	USA	1.6 X 1.3 m^2	Upper trench	Extensometer/Piezometer	30	Gravelly silty sand
		30 X 5 m^2			43	Weathered disintegrated granite sand
		3.2 X 4.0 m^2			70*	Coarse to medium grain sand with 20% clay
OCHIAI *et al.* 2004	Japan	30 X 5 m^2	Rainfall simulator	Extensometer/ Tensiometer/Strain probe/ Photogrammetry	33	Weathered disintegrated granite sand
TEYSSEIRE 2005	Switzerland	55 m^2	Rainfall simulator	TDR/Tensiometer/Moisture point	42	Moraine (Gravelly silty sand)
SPRINGMAN *et al.* 2012	Switzerland	130 m^3	Rainfall simulator	TDR/Tensiometer/ Piezometer/Soil deformation probe/ERT/ Soil pressure sensors/ Photogrammetry	38	Silty sand

ent of 33° (maximum 35°) located on a hill slope, by driving thin steel plates about 1 m deep into the soil. The plates prevented lateral percolation of infiltrated rainwater and reduced lateral tree root reinforcement. The surface material on the slope consisted of fine weathered disintegrated granite sand. The authors monitored the surface movements of the slope by means of photogrammetry video cameras. The depth of the shallow failure surface was detected using soil-strain probes, which were installed to a maximum depth of 2 m. The changes in the positive and negative pore water pressures were tracked by means of 6 tensiometers installed in the middle of the slope.

Artificial rain was sprinkled over the selected slope with 78 mm/h intensity for 4.5 hours for the first day, and no movements were measured. This first event was followed after 17 hours by a second one at the same intensity. First slope deformations were observed after 5.5 hours. Slope failure happened approximately 6.8 hours after the sprinkling was commenced. At this moment, a tension crack was observed on top and a compression zone at the bottom of the slope. The landslide liquefied and travelled at a speed of 3 m/s on a 10° gradient. The rate of compression straining in the lower part of the slope was calculated to be greater than the rate of extension straining in the upper part, based on photogrammetry results.

The tensiometers showed sequential increases in pore pressure according to the installation depth. The shallower tensiometers at depths of 0.50 and 1 m measured increases in pore water pressure and then they showed quite constant values. While, the deeper sensors (>1 m) measured sudden increases after the water front reached the corresponding depth and pore pressure did not attain a steady state condition with continuous increase until the final failure. This behaviour was attributed to the effect of the isolating longitudinal plates. However, it could also be an indication of the existence of preferential water paths in the shallower soil strata. The authors of the paper point to the coincidence of the arrival of the wetting front to the lowest tensiometer (depth of 2.90 m) with the acceleration of the bending strain at the depth of 1.10 m about 2 hours before the failure. This observation can be explained by the fact that the lowest tensiometer is installed at the interface of the soil mass and the bedrock, and arrival of the wetting front at this level might result in development of perched water table, which might favour further increase of the pore water pressure at shallower depth [KIENZLER, 2007]. This hypothesis could be supported by the change in rate of increase in pore water pressure measured by the tensiometers at depth of 1.0 and 1.5 m (which are installed near the eventual shear surface), approximately 2 hours before the failure.

TEYSSEIRE [2005] selected a 42° steep alpine moraine slope, at about 2800 m above sea level (masl) in the forefield of the Gruben glacier (Canton Wallis, Switzerland) as a field test site. It was instrumented over a 55 m^2 plan area for an artificial rainfall test in summer 2000, to investigate slope stability in moraine as a function of degree of saturation and relative density of the soil.

A series of insitu direct shear box tests, of plan area 250 mm x 250 mm, was carried out at the field test-site on samples that were carved out of the unsaturated ground. The specimens exhibited dilatancy at failure. The internal friction angle for this soil, based on the gradient of the peak shear strength envelope, was $\varphi' = 41°$ [SPRINGMAN *et al.,* 2003].

Rainfall was applied for 50 hours with an average intensity of 16 mm/h for the first day and 12 mm/h for the second day. The slope failed after ~2 days, and the sprinkling was stopped. Instability occurred in the slope when S_r approached 0.95. The slip surface was located at the depth of approximately 0.2 m. Time Domain Reflectometers (TDRs) installed at depths of 0.19 and 0.12 m show a decrease in the degree of saturation at approximately 6 and 1.5 hours before the failure, respectively. This observation is similar to the results of HARP *et al.* [1990] and can be attributed to the dilation of the soil elements along the shear surface. This hypothesis might be supported by the fact that the drop in the degree of saturation measured at depth of 0.19 m, which is the nearest sensor to the failure surface, was more pronounced [ASKARINEJAD *et al.,* 2010b].

ALONSO *et al.* [2003] performed a series of coupled hydro-mechanical simulations to analyse the behaviour of an instrumented unstable slope in eastern Italy in terms of slope motions, variation of safety factor, and their relationship with rainfall. The investigated slope is composed of three partially saturated overconsolidated clay layers. The authors showed that changes between layers might result in high pressures at the interfaces of layers. These peak pressures decrease the factor of safety and enhance the strains. Accumulated strains might promote the strength degradation lead to movements developping at the interfaces. Accordingly, they lead to conclude that the hydraulic properties of the soil profile play a major role in the stability of layered slopes.

NG and SHI [1998] performed a parametric study using finite element method to analyse the stability of unsaturated slopes due to rainfall. They found out that not only the intensity of the rainfall event, but also the initial ground water level and duration of the rain play, major roles on the stability of the slopes.

Despite prior research, there is still a lack of knowledge on some aspects, such as the stabilising effects of vegetation, the influences of bedrock shape, the regional hydrogeological properties, and all are linked to the hydro-mechanical behaviour of the overlying unsaturated soil.

This project was conducted within the context of a multi-disciplinary research programme on Triggering of RApid Mass Movements in steep terrain (TRAMM[1]). The primary focus of this research is to enhance the understanding of triggering and initiation mechanisms, including the transition from slow to fast mass movement processes, and flow characteristics of such catastrophic mass movements. The influence of rainfall events on slope stability is investigated by monitoring a natural slope in Ruedlingen, Switzerland. The hydro-mechanical responses of the slope were studied under natural and artificial atmospheric conditions. These results are used to calibrate models adopted to predict possible landslides in the future.

The characteristics of the experiment field in terms of the topography, geology and hydrogeology and the shape of the bedrock, hydrological properties of the soil mass, the instrumentation plan and the saturated and unsaturated hydro-mechanical properties of the soil are discussed. The responses of the slope to two intense artificial rainfall events (October 2008, and March 2009) are discussed next. The first experiment, (October 2008) despite having a more intense rainfall and longer duration, did not result in triggering a landslide. However, in the second experiment (March 2009) a landslide of 130 m^3 was mobilised after 15 hours of rainfall. The difference between the two experiments was in the location of the rain concentration (rain was more intense at the places were the bedrock was shallower and less vegetation effects were expected in the second experiment). In the next section of the paper, simplified 2 and 3 dimensional limit equilibrium methods are implemented to investigate the effect of the side walls of the failure wedge and also the roots reinforcement on the changes of the factor of safety of a slope subjected to rainfall. Finite element program was used to simulate the changes in the pore water pressure during the rainfall and the results are compared to the in situ measurements. The effects of the vegetation on the evolution of the factor of safety are also studied.

2. Experiment field

2.1. Location and geometry

The experiment field was chosen in a forested area near Ruedlingen village, which is located in northern Switzerland. Following an extreme event in May 2002, in which 100 mm of rain had fallen in 40 minutes, 42 surficial landslides occurred around the local area [FISCHER *et al.,* 2003]. The selected

[1] http://www.cces.ethz.ch/projects/hazri/tramm

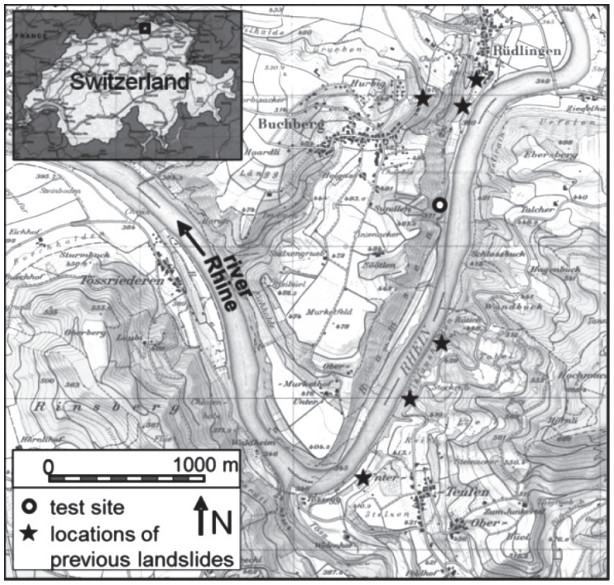

Fig. 1 – Location of the test site, detailed map and map of Switzerland [after SIEBER, 2003].
Fig. 1 – Ubicazione del sito di prova, mappa dettagliata e mappa della Svizzera [da SIEBER, 2003].

experimental site of 35 m length and 7.5 m width is a small part of a slope on the east facing bank along the river Rhine. Figure 1 shows the location of the test site and previous landslides. The altitude is about 350 masl. The average gradient of the slope was determined using a total station theodolite to be 38° with maximum of 43° in the middle of the slope. The surface of the slope is slightly concave; the longitudinal centreline is 0.3 to 0.5 m lower than the sides (Fig. 3).

2.2. Geology and the bedrock shape

The site is located in the Swiss lowlands. The geological progression consists mainly of Molasse, which is the sediment that was deposited in the foreland basin of the Alps, containing alternate depositions in the Tethys Sea (Seawater Molasse) and on land (Freshwater Molasse) (Fig. 2). Several boreholes, as well as an outcrop of bedrock about 20 m above the selected field, revealed horizontal layering of the sedimentary rocks at the experimental slope, which consisted of fine grained sand- and marlstone [TACHER and LOCHER, 2008]. Fissures with openings of more than some centimetres in size were mapped in the lower freshwater molasse, and were parallel to the Rhine [BRÖNNIMANN *et al.*, 2009].

Dynamic probing tests were performed every 2 m around and across the middle of the field in order to locate the depth of bedrock. The probing was done with the Dynamic Probing Light method (DPL), which operates with a 10 kg weight, dropped over 0.5 m, generating energy of 50 kJ to drive rods and a cone into the ground. The cone diameter is d = 35.7 mm (cross section: 1000 mm^2), tip angle 90° [DIN 4094]. The penetration rate of the cone allows the mechanical resistance of the soil to be evaluated empirically. The number of required blows for each 0.1 m was counted, and the criterion for the underlying bedrock was set as 30 blows per 0.1 m penetration.

According to the DPL results, the bedrock level lies between 0.5 m to more than 5 m depth. Bedrock on the right hand side of the field (P3-M2-P4) is shallower than on the left (P2-M1-P1; Fig. 3). The shallow convex feature located between M1-M2 and P1-P4 may be due to the accumulation of older landslide materials. The gradient of the slope is about 25° at this point.

These results agree well with those obtained from extensive geophysical Electrical Resistivity Tomography (ERT) surveys [GAMBAZZI and SUSKI, 2009], although post slide excavation revealed the presence of stones embedded in the matrix of the overlying soil (possible former debris), which could have implied that bedrock had been reached at a shallower depth than was actually the case.

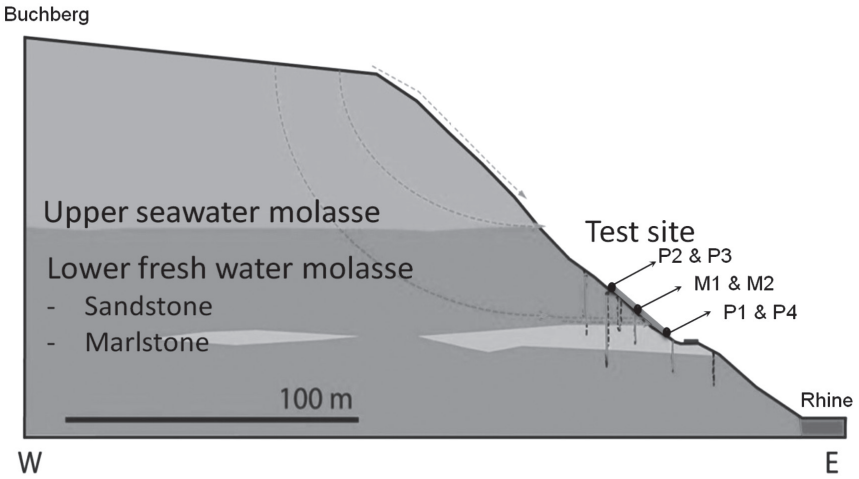

Fig. 2 – The geological lithology of the test site [after BRÖNNIMANN *et al.*, 2009].
Fig. 2 – Litologia del sito di prova [da BRÖNNIMANN et al., 2009].

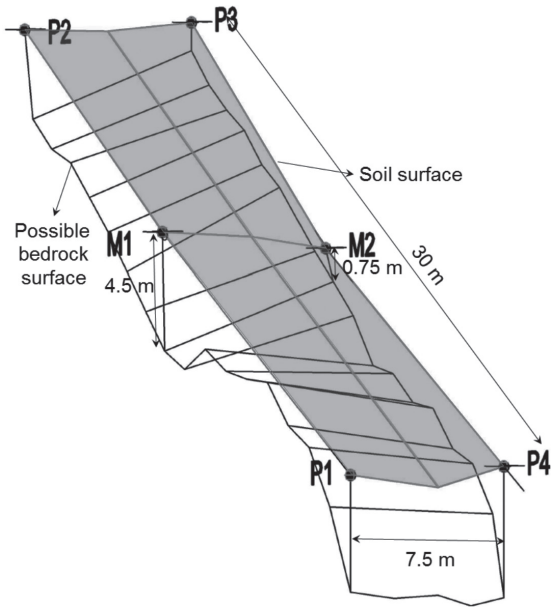

Fig. 3 – The 3D shape of the bedrock based on DPL results.
Fig. 3 – Mappa 3D del substrato roccioso in base ai risultati DPL.

Electrical Resistivity Tomography (ERT) provides a tool for measuring and high quality imaging electrical resistivity in soil. Decreases in the electrical resistivity during a rainfall event can be due to increases in the degree of saturation. ERT measurements were performed along the left and right longitudinal sections of the slope in the first experiment in October 2008, and March 2009, respectively [LEHMANN *et al.,* 2012]. The ERT measurements were conducted every 30 minutes during the artificial rainfall events applied in both experiments. The considerable changes in the resistivity (from more than 140 ohm.m to 20 ohm.m) at some localised points in the bedrock during the course of the rainfall can be an indication of the location of fissures. Several fissures in the bedrock have been recognised based on hydrogeological investigations before the monitoring experiment and tracking the changes of the electrical resistivity of the slope during the experiment.

2.3. Hydrology

Three sets of combined sprinkling and dye tracer tests were performed at different locations near the experiment slope to characterise the hydrological properties of the soil profile [KIENZLER, 2007]. These tests were done through sprinkling dyed water with uniform intensity of 60 mm/h over a confined circular area of 1 m^2 (Fig. 4a). Runoff was measured using a 100 ml tipping bucket. Brilliant Blue FCF food dye was added in a concentration of 4 g l^{-1} to the sprinkling water to visualise infiltration flow paths [SPRINGMAN *et al.,* 2009]. Three vertical sections with spacing of 0.15 to 0.2 m, and depth of 1.2 m were excavated about 24 hours after the sprinkling had stopped.

Dye patterns (Fig. 4b) were analysed according to WEILER and NAEF [2003]. The dye patterns showed a mixture of preferential drainage along the roots combined with more homogeneous wetting in some locations. Evidence was noted of partial perched saturation above the sandstone bedrock. However, stained fractures below the subsoil (Fig. 4c), revealed that substantial drainage

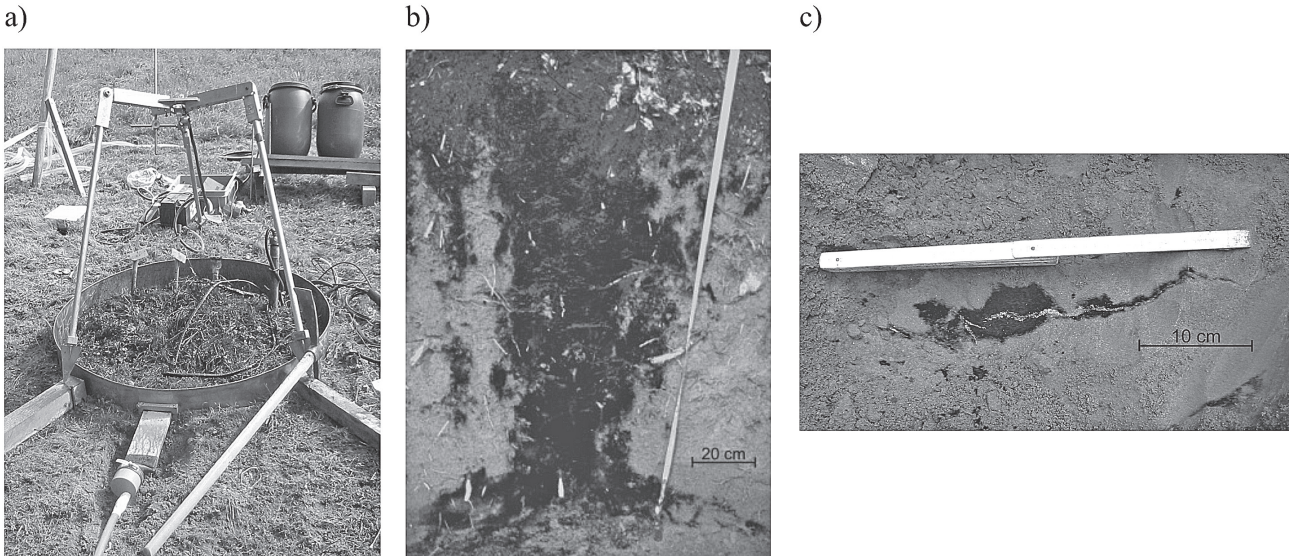

Fig. 4 – a) Small-scale sprinkling apparatus for the combined sprinkling and dye tracer experiments; b) Dye pattern; c) Stained fracture in the weathered bedrock below the subsoil [SPRINGMAN *et al.,* 2009, photos: P. Kienzler].
Fig. 4 – a) Attrezzatura utilizzata su piccola scala per le prove di pioggia artificiale costituita da fluido colorante blu; b) Percorso del colorante; c) Frattura nel substrato roccioso raggiunta dal fluido colorante [SPRINGMAN et al., 2009; photo: P. Kienzler].

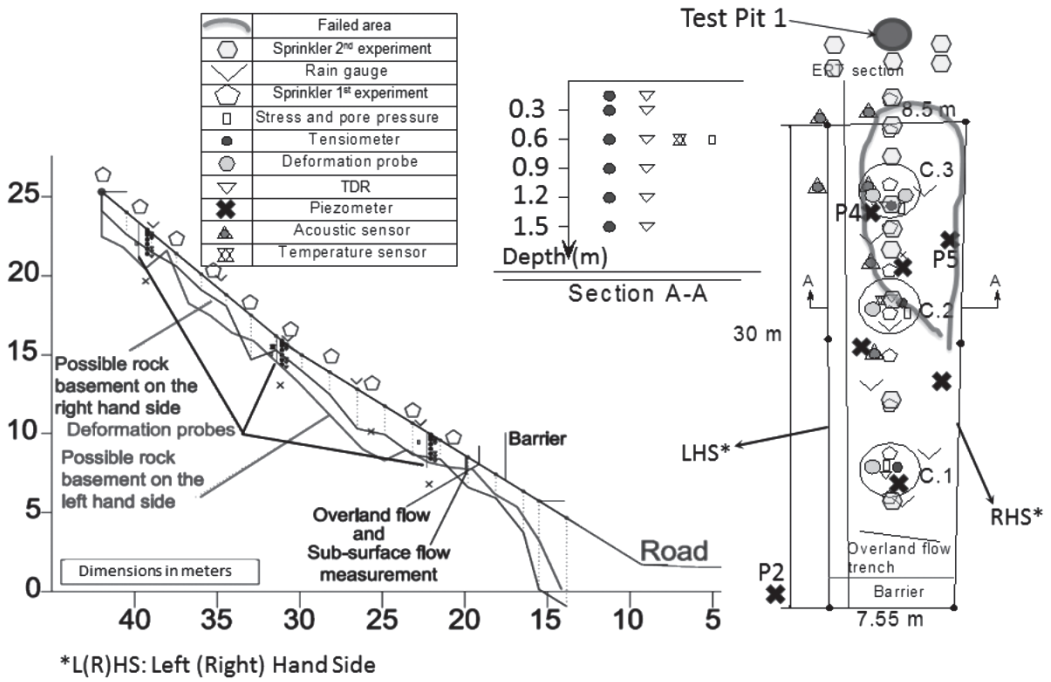

Fig. 5 – The bedrock topography and the instrumentation plan [ASKARINEJAD *et al.,* 2010b].
Fig. 5 – Topografia in pianta del substrato roccioso e della strumentazione [ASKARINEJAD et al.*, 2010b].*

might occur into the bedrock, which may prevent complete saturation and failure of the experimental slope [KIENZLER, 2008]. No runoff was observed during the sprinkling at any of the three locations [SPRINGMAN *et al.,* 2009].

2.4. Instrumentation

The slope was instrumented to monitor the hydrological and geo-mechanical responses of the soil and bedrock during the rainfall events. Detailed measurements of positive and negative pore water pressures (using tensiometers), piezometric water level (using piezometers) and soil volumetric water content (using TDRs), subsurface flow and runoff were performed. Deformations were monitored during the experiment, both on the surface using photogrammetrical methods and within the soil mass, using a flexible inclinometer equipped with strain gauges at different points and two axis inclinometers on the top [ASKARINEJAD, 2009].

The instruments were installed mainly in three clusters over the slope. Each cluster included a soil temperature sensor at depth of 0.6 m, deformation probes, earth pressure cells, acoustic sensors and rain gauges (Fig. 5). The tensiometers were installed at depths of 0.15, 0.3, 0.6, 0.9, 1.2, and 1.5 m in each cluster and were collocated, as much as possible at each depth, with TDRs at 0.15 m, and from 0.3 m to 1.5 m, with a spacing of 0.3 m.

All the instruments were calibrated and checked in the laboratory that they functioned correctly before installation in the field. The hydrological response of the soil was measured during the experiment with a logging interval of 5 minutes, while the subsurface deformations and the horizontal soil pressures were measured at a frequency of 100 Hz.

The artificial rainfall was applied by means of 10 sprinklers located at the same spacing on the middle longitudinal line of the field in the first experiment (Fig. 5). Lower sprinklers experienced higher hydraulic heads as water was supplied from above the slope and so rainfall was not uniformly distributed. The rain intensity at the lower part of the slope (where larger fissures were detected and bedrock was deeper) was higher than at the top of the slope.

Accordingly, the sprinklers were rearranged for the second experiment. The spacing between the lower sprinklers was increased and 4 more sprinklers were added to provide more rainwater to the upper part of the slope where less root reinforcement and shallower bedrock was expected (plan view in Fig. 5).

3. Soil characterisation

3.1. Soil classification

Soil samples were collected from test pits (TPs) at different depths. The grain size distribution, the natural water content, together with consistency limits and activity, are shown with depth for the time of sampling for TP1 in the upper part of the slope. The data for TP1 may be considered to be representative of the whole test site.

The soil can be classified as medium to low plasticity silty sand (ML) according to USCS. Activity of

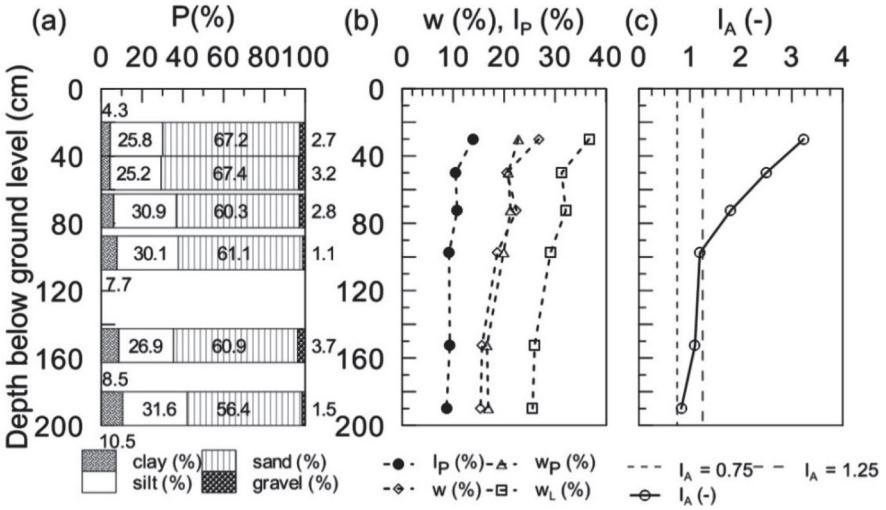

Fig. 6 – Basic properties with depth : (a) Grain size distribution ; (b) Gravimetric water content, Atterberg limits and plasticity index ; (c) Activity index (after Casini *et al.,* 2010a).

Fig. 6 – Proprietà di base con la profondità: (a) Distribuzione granulometrica; (b) Contenuto gravimetrico d'acqua, limiti di Atterberg e indice di plasticità; (c) Indice di attività (da Casini et al., 2010a).

the soil is derived from the chloritic-smectitic clay fraction [Colombo, 2009]. The activity, I_A, is higher than 1.25 in the upper part of the soil profile and decreases from I_A = 1.25 to I_A = 0.75 below 1 m depth. The clay fraction increases with depth from 4% at shallow depths to 10% at about 2 m. The silt fraction also increases with depth from 25% to 32%, while the sand fraction decreases from 67% to 56% (Fig. 6). The increase of the fine fraction with depth may be due to internal erosion induced by sedimentological and morphological reasons, and downward transport promoted by infiltrating water, flushing the fines into the larger voids surrounding the peds [Casini *et al.,* 2010a].

As the relevant properties of the soil are mostly influenced by the fines content, undisturbed samples from different depths, with various fines content, were tested in the laboratory experimental programme presented in the following section [Casini *et al.,* 2010a].

3.2. Laboratory tests

An extensive soil investigation was conducted to understand how the strength is mobilised in the soil and how this may be related to change in water content and void ratio in the slope. The investigation includes tests on both undisturbed and reconstituted soil samples. Water retention characteristics and hydraulic conductivity have been investigated. Oedometer tests, in situ shear tests, laboratory tests with a standard shear and a modified shear apparatus have been performed as well as triaxial tests on saturated and unsaturated soil samples [Springman *et al.,* 2009; Colombo, 2009; Casini *et al,*. 2010 a-b].

The parameters obtained from oedometer tests on natural samples (oedNS) and shear tests on statically compacted samples (shSC) are summarised in Table II.

Tab. II – Parameters obtained from laboratory results.
Tab. II – Parametri ottenuti dalle prove di laboratorio.

	c' (kPa)	φ' (°)	C_c (-)	C_s (-)	σ'_{v_max} (kPa)
oedNS ($w = w_{sat}$)	-	-	0.25	0.016	40
oedNS (w = 0.20)	-	-	0.14	0.012	80
shSC (Bishop stress)	0	31	-	-	-

3.2.1. Triaxial tests

Isotropic and anisotropic drained compression tests were performed to different stress ratios, both to replicate the in situ stress state and to analyse the dependence of volumetric stiffness on the stress ratio [Casini *et al.,* 2010a]. After volumetric compression, failure was approached following a range of suitable stress paths under different drainage conditions.

Standard drained (CIDC) and undrained (CIUC) shear compression tests were performed, together with constant axial load shear compression tests under decreasing isotropic stress due to the increase of pore water pressure. In the latter case, both drained (CADCAF) and undrained (CADCAUF) conditions were studied after an initial drained stage, to analyse the influence of the hydraulic boundary conditions on the eventual failure mechanism of the soil specimens [Casini *et al,*. 2010a]. The data collected are reported in terms of:

$$p' = 1/3\ (\sigma_a + 2\sigma_r);\ q = \sigma_a - \sigma_r;\ p' = p - u;\ \eta = q/p';\quad (1)$$

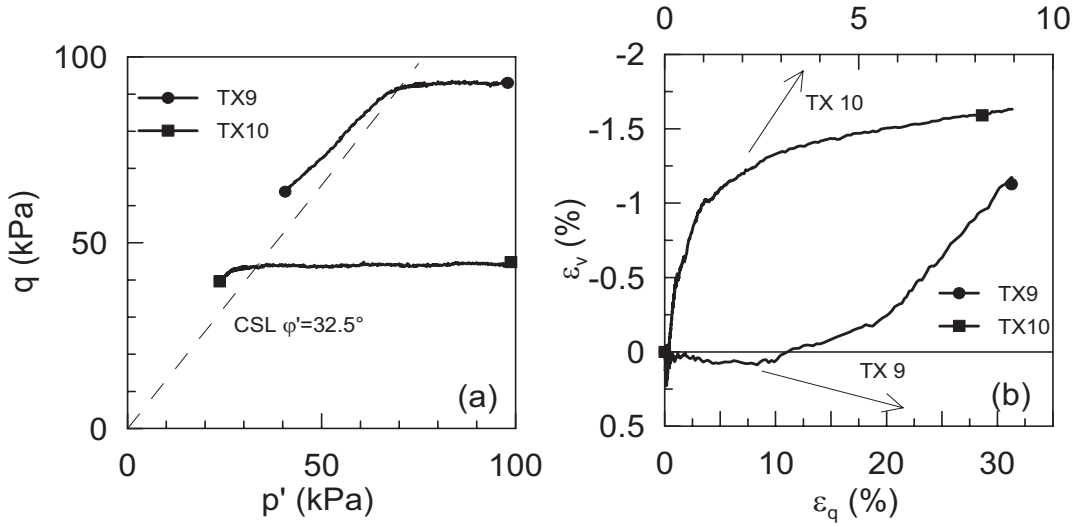

Fig. 7 – CADCAF results: (a) p'-q plane; (b) $\varepsilon_q - \varepsilon_v$ plane, with strain axes at the top for TX10 and bottom for TX9 [CASINI *et al.*, 2010a].

Fig. 7 – Risultati di prove CADCAF nei piani: a) p'-q ; (b) $\varepsilon_q - \varepsilon_v$ [CASINI et al., *2010a].*

$$\varepsilon_q = 2/3\ (\varepsilon_a - \varepsilon_r);\ \varepsilon_v = \varepsilon_a + 2\varepsilon_r;\ \Delta u = u - u_0 \qquad (2)$$

where σ_a is the axial total stress and σ_r is the radial total stress applied in the triaxial cell under axisymmetric conditions. Pore water pressure u is measured in both the upper and lower platens, u_0 is the initial pore water pressure. Axial strain is defined as $\varepsilon_a = \Delta h / h_0$ where h_0 is the initial height of the specimen prior to shearing and Δh was measured over the entire specimen length. Volumetric strain $\varepsilon_v = \Delta V / V_0$ was deduced from water exchange into or out of the specimen, where ΔV is the volume change and V_0 is the corresponding initial volume prior to shearing. Conventionally, radial strain was derived as $\varepsilon_r = (\varepsilon_v - \varepsilon_a)/2$. Deviatoric stress is defined as $q = \sigma_a - \sigma_r = F/A$, where F is the axial force and A is the current cross-sectional area of the specimen, corrected by assuming it remained as a right cylinder [HEAD, 1998].

The results for the CIDC and CIUC tests, plotted all together in the $\varepsilon_q - \eta$ plane, were exploited to detect a possible critical state stress ratio. In spite of the data variability, typical of natural samples, a value of $\eta_{CS} = 1.30$, corresponding to a critical state friction angle of about $\varphi'_{cs} = 32.5°$, seems to represent the critical state conditions for this soil. The CADCAF results are reported in figure 7. Specimens TX9 and TX10 were anisotropically compressed until to $p' \approx 100$ *kPa* with $\eta = 0.95$ and $\eta = 0.44$ respectively. Increasing the pore water pressure promotes a slight increase in the void ratio for TX9, which is likely to be the result of elastic swelling as the stress path moves inside the yield locus. Slightly after the critical state stress ratio, a definite increase in shear strain was observed, together with a further sudden increase in volumetric strain. The data, which will be discussed in more detail in the following section, already highlight the stress ratio (e.g. $\eta = q/p' \geq 1.4$) at which an instability mechanism occurred. The sudden increase in volume is the evidence of a dilatant failure mode with plastic volume increase.

The difference in friction angle between shear tests (statically compacted sample) and triaxial tests (natural sample) may be due to the different type of test [NOCILLA *et al.*, 2006; HAN and VARDOULAKIS, 1991].

3.3. Saturated and unsaturated hydraulic conductivities

The hydraulic conductivity measurements are carried out based on the instantaneous profile method [DANIEL, 1982]. This method consists of measuring the variation of the suction and volumetric water content profile within an infiltration column as a function of time during the infiltration process. Accordingly, an infiltration column was developed with a height of 600 mm and an inner diameter of 170 mm. The suction and volumetric water content were measured simultaneously every 100 mm in depth by 3 mm diameter tensiometers and TDRs, respectively. These measurements provide enough data to correlate the hydraulic conductivity with the negative pore water pressure and/or degree of saturation. The change in the height of the soil sample during the flow of water is monitored using a set of LVDTs on the upper part of the soil column, enabling the volumetric changes to be tracked during the test. The tests are performed on statically compacted soils with different initial void ratios. The configuration of the tests is illustrated in figure 8.

Based on Darcy's law (Eq. 3), the hydraulic conductivity k is calculated by dividing the water flow velocity by the hydraulic gradient.

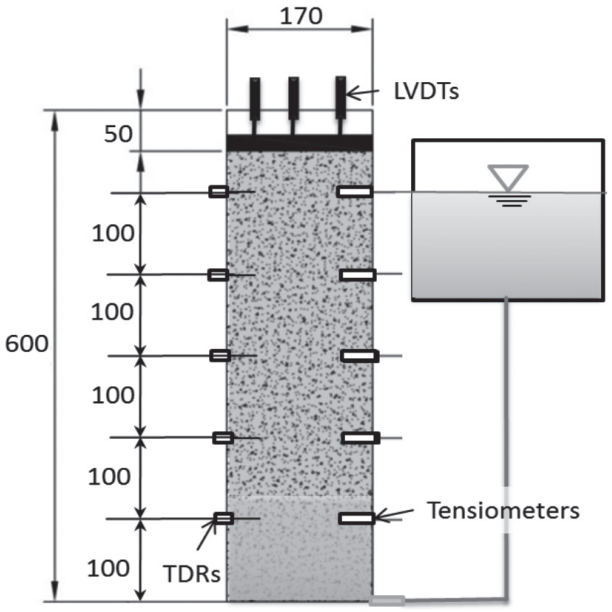

Fig. 8 – Infiltration column (dimensions in mm).
Fig. 8 – Colonna di infiltrazione (dimensioni in mm).

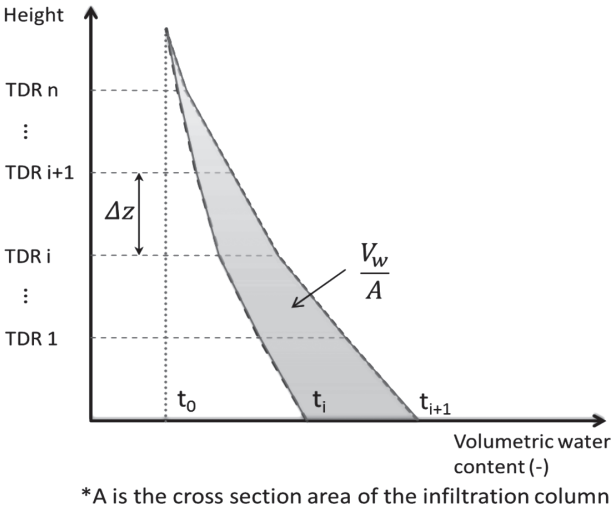

Fig. 9 – Schematic of water content distribution through the infiltration column.
Fig. 9 – Rappresentazione schematica della distribuzione del contenuto in acqua nella colonna di infiltrazione.

$$k = -\frac{v}{i} \tag{3}$$

where k is the hydraulic conductivity (m/s), v is the velocity of water flow (m/s) and i is the hydraulic gradient.

The water flow velocity v is defined as the volume of water flow passing through the whole cross-sectional area over a given time increment (Eq. 4):

$$v = \frac{V_w}{A\Delta t} \tag{4}$$

where A is the cross-sectional area (m^2) of the infiltration column, V_w is the volume of water flowing through the column (m^3) and Δt is the time required for the flow (s).

Combining equations (3) and (4), the unsaturated hydraulic conductivity can be calculated based on the measured pore water pressure and changes in the profile volumetric water content.

$$k = \frac{V_w}{A\Delta ti} \tag{5}$$

The hydraulic gradient (i) can be calculated using Equation (6) for an upward water flow.

$$i_i = \frac{(H_{p,i} + H_{e,i}) - (H_{p,i+1} + H_{e,i+1})}{\Delta z} = \\ = \frac{(H_{p,i} - H_{p,i+1})}{\Delta z} \tag{6}$$

where, i_i is the hydraulic gradient at point i, $H_{p,i}$ is the pressure head at point i, $H_{e,i}$ is the elevation head of point i and Δz is the vertical distance between the points i and $i+1$. Accordingly, the suction profile in the soil is needed in order to calculate the hydraulic gradient between different elevations.

The volume of water passing through any cross-sectional area over a given time increment is equal to the change in the volume of water occurring between the point i under consideration and the top of the specimen (Fig. 9). This volume can be calculated using a trapezoidal rule based on the volumetric water contents measured by the TDRs at different heights between two different times:

$$V_w = A\sum_{1}^{n}\left(\frac{(\theta_{i+1}(t_2) + \theta_i(t_2)}{2} - \frac{(\theta_{i+1}(t_1) + \theta_i(t_1)}{2}\right)\Delta z \tag{7}$$

where $\theta_i(t_j)$ is the volumetric water content at point i and time j, and n is the number of TDRs.

The changes in the pore water pressure and volumetric water content are measured simultaneously during these tests and a water retention curve could be derived, based on these results (Fig. 10a).

The saturated conductivity is measured to be about 10^{-6} m/s (Fig. 10b). This value is lower than the in-situ measurements of hydraulic conductivity performed using the inversed auger-hole method [OOSTERBAAN and NIJLAND, 1994]. The in-situ measured hydraulic conductivity varies between 10^{-4} to 10^{-5} m/s [BRÖNNIMANN *et al.*, 2009]. The inconsistency between the laboratory and *in situ* measurement can be explained by the influence of the difference in micro- and macro-porosities in the reconstituted soil and the natural soil. The hydraulic conductivity of Ruedlingen soil decreases by two orders of magnitude with 40 kPa increase in the suction (Fig. 10b).

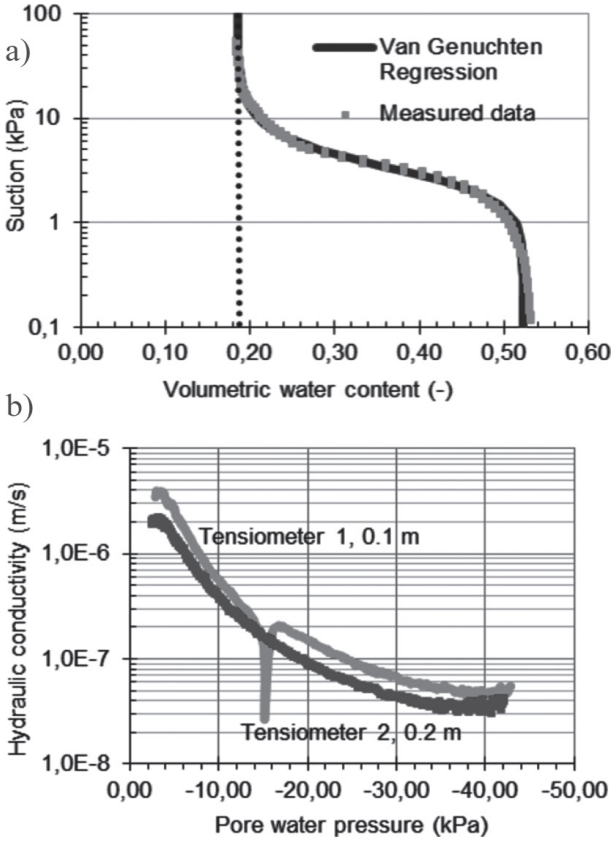

Fig. 10 – a) Water retention curve derived from the infiltration process (e = 1.0); b) Unsaturated hydraulic conductivity of the Ruedlingen soil (e = 1.0) [BECK, 2010].

Fig. 10 – a) Curva di ritenzione idrica ottenuta da una prova di infiltrazione (e = 1.0); b) Permeabilità non satura del terreno di Ruedlingen (e = 1.0) [BECK, 2010].

4. Slope monitoring experiment

4.1. Rainfall

The applied rain intensity is shown in figure 11a, with an average value of 35 mm/hr for 3 hours as the first wetting phase (W1), followed by a pause for 20 hours to allow the soil to drain (first drying phase – D1). The slope was then sprinkled for 1.5 days with an average intensity of 17 mm/hr, which increased after a brief shock of 45 mm/hr to average 30 mm/hr for another 1.5 days (second wetting phase – W2). The second drying phase was then started (D2). The total amount of rain sprinkled over the slope within 4.5 days was approximately the total average rainfall for two years in this region [ASKARINEJAD *et al.,* 2010a].

4.2. Hydro-mechanical behaviour of slope

No failure was observed in the slope after 4.5 days of rainfall although the tensiometers showed positive pore pressures, mainly at depths from 0.9 to 1.5 m. The piezometers inside and outside the sprinkled area showed small increases in the water table (maximum of 0.2 m) and this water table drained very fast after the rainfall stopped. The fast drainage and the reaction of the piezometer located outside of the sprinkled area (P2 in Fig. 5) indicate the existence of an interconnected system of fissures in the bedrock in the lower part of the slope.

Movements were concentrated in the upper right quarter of the field (looking from downslope), according to the photogrammetric analysis, after comparing photographs taken from the first and last days of rainfall. Maximum displacements were around 15 mm (Fig. 12), and the order of magnitude agreed well with values measured by soil deformation probes [ASKARINEJAD, 2009].

5. Landslide triggering experiment

The maximum displacements were observed to be in the upper right part of the field during the first experiment, where shallower (Fig. 5) and more intact bedrock [SPRINGMAN *et al.,* 2009], and less root

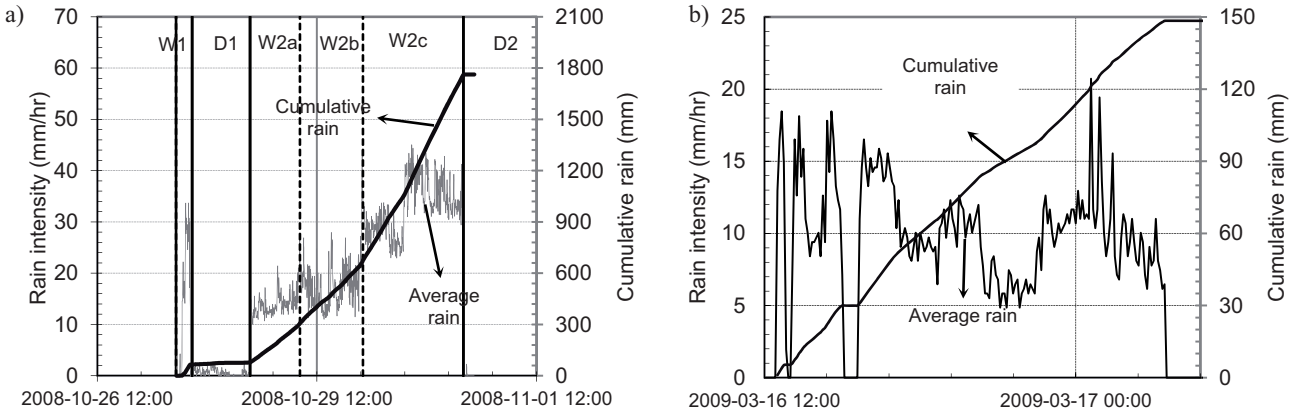

Fig. 11 – a) Average and cumulative rainfall in the monitoring experiment (October 2008); b) Average and cumulative rainfall in the triggering experiment (March 2009).

Fig. 11 – a) Pioggia media e cumulata durante l'esperimento di monitoraggio (ottobre 2008); b) Pioggia media e cumulata durante l'esperimento a rottura (marzo 2009).

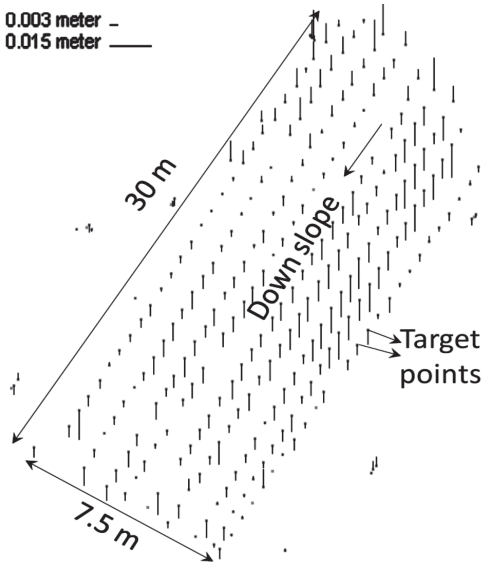

Fig. 12 – The vertical component of displacements between the 28 and 31 October 2008 [AKCA *et al.,* 2011].
Fig. 12 – Componente verticale degli spostamenti misurata tra il 28 e il 31 ottobre 2008 [AKCA et al.*, 2011].*

reinforcement were expected [SCHWARZ and RICKLI, 2008]. Accordingly, it was decided to concentrate the rainfall on the upper part of the slope for the second experiment. Furthermore, the lateral roots along the longitudinal borders of the field were severed up to the maximum depth of 0.4 m in order to reduce the lateral reinforcement from the vegetation.

5.1. Rainfall

The 10 sprinklers from the first experiment and 4 additional ones were re-arranged with variable spacing that was selected to provide more intense rainfall to the upper part of the slope and was adjusted to supply an average intensity between 10 to 15 mm/h (Fig. 11b).

5.2. Changes in volumetric water content

Figure 13a shows the changes in Volumetric Water Content (VWC) during the experiment. The initial values of the VWC are between 27% (at depths of 0.6 and 1.2 m) to 35% (at depths of 0.9 and 1.5 m). This difference in the initial value can be due to the difference in the porosity and/or degree of saturation of various locations along the soil profile. The shallowest TDR at depth of 0.6 m reacted shortly after the start of the rainfall and the other TDRs showed increases in the VWC sequentially according to their installation depths. The VWC at depths of 0.6, 0.9, and 1.5 m increased due to the rain and remained quite constant until the failure and only the TDR of 0.6 m measured a decrease of 2% after the rain was stopped for approximately one hour. However, the TDR installed at the depth of 1.2 m, showed a dynamic response to the changes in the rainfall. This sensor also measured higher values of VWC, after complete saturation, compared to the other TDRs installed at other depths. This might be an indication of the existence of a more porous layer at this depth which is well connected via preferential water paths to the shallower depths. This TDR (at the depth of 1.2 m), which was the nearest instrument to the eventual slip surface measured a decrease in water content about 1 hour before the failure (Fig. 13a) [ASKARINEJAD *et al.,* 2010b].

The piezometers P4 and P5 (shown in Fig. 5), which were located inside the eventual failure zone, also showed a decrease in the piezometric level (Fig. 13b) [ASKARINEJAD *et al.,* 2010b]. Piezometer P4 is installed at the depth of 3 m from the slope surface and showed a faster reaction to the start of rainfall. It attained a higher value compared to P5. This behaviour can be explained by the fact that this piezometer was installed in higher location where more intense rainfall was provided to the slope. Moreover, the gap between the casing and the borehole wall of the piezometer P4 was filled with gravel which makes the sensor act as a "*well*" rather than a local piezometer. The observed decrease in the piezometric levels was more pronounced in P5 (approximately 0.12 m) which was nearer to the failure surface. The decrease time corresponds well to the time when VWC at 1.2 m also slightly decreased (about 1 hour before the landslide).

These observed decreases in the VWC and piezometric level at the failure surface before the landslide is triggered can be attributed to the dilation of the soil at the failure surface or piping of the fine grained material. Dilation has been observed in the representative CADCAF triaxial tests performed on the undisturbed samples from the same soil (Fig. 7b).

The sudden drops in the measurements at the ending part of the graphs in figures 13(a-b) are due to the breakage of the cables and lack of connection between the sensors and the data logger after the failure.

5.3. Surface movements and the failure wedge

Based on the photogrammetric measurements [AKCA *et al.,* 2011], increasing downslope movements started about 2 hours before the failure in the middle and upper parts of the slope (Fig. 14a). The velocity of movements at cluster 3 (top) is higher than in the middle and at the bottom. The movements start to accelerate about 30 minutes before the failure and stepwise movements were measured during this period (Fig. 14b). These stepwise movements

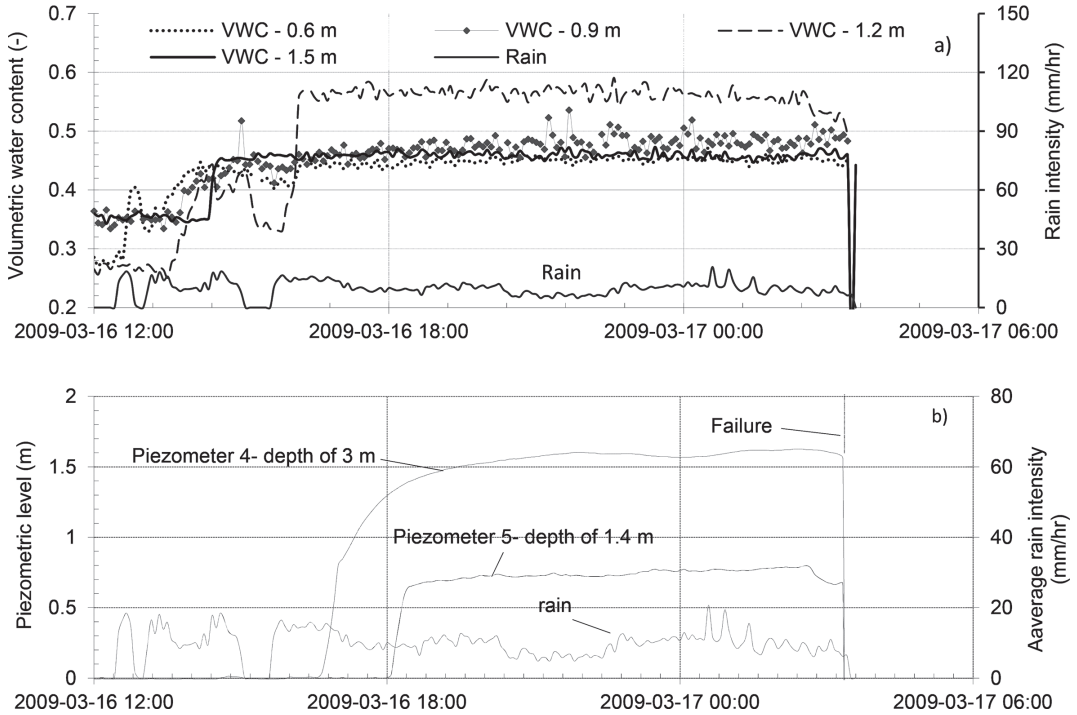

Fig. 13 – a) Changes in the volumetric water content profile in cluster 3; b) Changes in the piezometric level at two points on the upper part of the slope (after ASKARINEJAD *et al.*, 2010b).

Fig. 13 – a) Evoluzione del contenuto volumetrico di acqua nel cluster 3; b) Evoluzione della altezza piezometrica in due punti diversi nella parte alta del pendio (da ASKARINEJAD et al.*, 2010b).*

occurred perhaps because ofthe pull out or breakage of the roots and/or the dilative behaviour of the soil mass in the shear band. As illustrated in figure 13 and discussed in 5.2, drops in the water content and piezometric level in the vicinity of the failure surface were recorded. These observations support a hypothesis of dilative behaviour of the soil or drainage through tension cracks developing just prior to slope failure.

Some seconds before tension cracks appeared across the top of sprinkled area, the right side of the landslide followed the line along which the roots were cut (Fig. 15). It took about 36 seconds to mobilise about 130 m^3 of debris. The water was exfiltrating from the back of the scarp after the failure (Fig. 15). The places where water oozed out from the bedrock were mainly located on the upper right part of the slope. They can be indications of interconnected

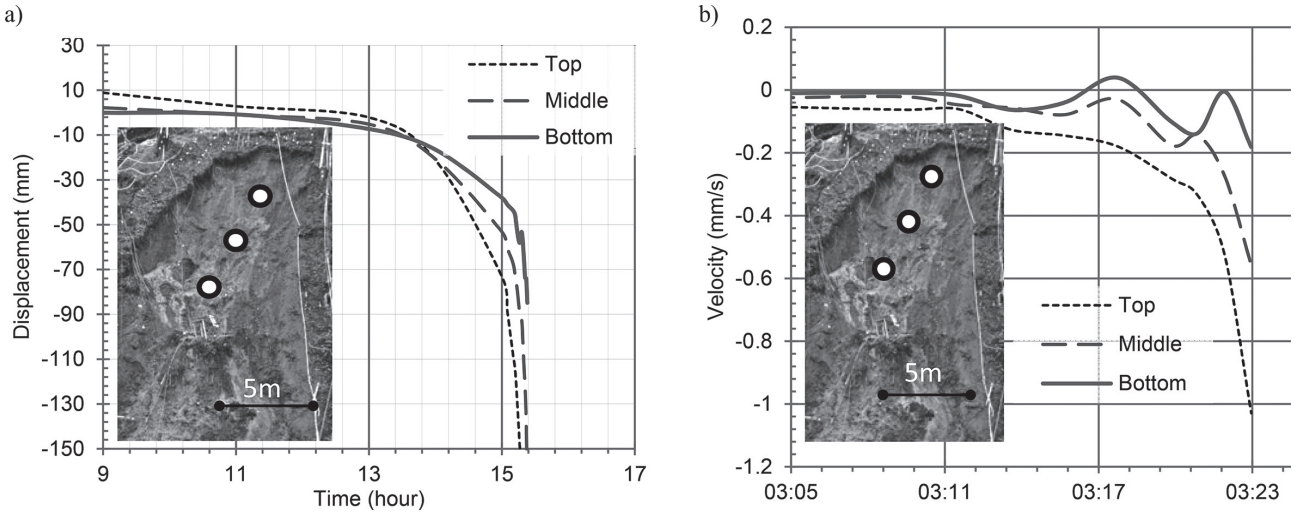

Fig. 14 – a) The surface movements in the Z direction at three points on the failure wedge (time 0, is the start of the rainfall); b) The changes in the velocity in the Z direction during 20 minutes before the failure (the coordinate system is shown in Fig. 20).

Fig. 14 – a) Movimenti superficiali in direzione Z in tre punti diversi nel cuneo di rottura (tempo 0, è l'inizio delle precipitazioni); b) Evoluzione della velocità in direzione Z durante i 20 minuti precedenti la rottura (il sistema di coordinate è mostrato in Fig. 20).

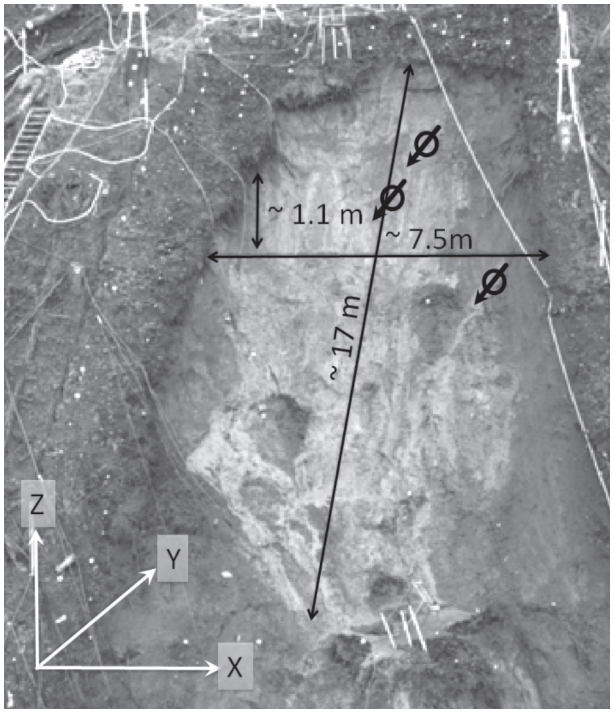

Fig. 15 – Shape of the failure wedge and locations of water outflow after the failure.
Fig. 15 – Forma del cuneo di rottura e punti di fuoriuscita dell'acqua dopo la rottura.

permeable layers, which transferred the water from the upper parts of the slope to these locations. This water flow applied an outward seepage force to the soil mass and functioned as a key triggering factor for the landslide.

6. Analytical limit equilibrium simulations

6.1. 2D infinite and 3D slope analysis

The equation for factor of safety has been derived for the infinite slope model, assuming a shallow, translational soil movement along a planar surface parallel to the ground. In this equation, the shear strength of the soil is based on the effective stresses proposed by BISHOP [1959] for unsaturated soils.

$$\sigma' = (\sigma - u_a) + \chi(u_a - u_w) \tag{8}$$

where σ' is the effective stress, σ is total stress, u_a is pore air pressure, u_w is pore water pressure, the quantity $s = (u_a - u_w)$ is matric suction, and χ is a material property that depends on the degree of saturation or matric suction.

In this section, it is assumed that:

$$\chi = S_r \tag{9}$$

where S_r is the degree of saturation.

Bishop's effective stress with, $\chi = S_r$ will change to the saturated effective stress [TERZAGHI, 1936] if the pore pressures at the slip surface become positive. Nonetheless, the slip surface is presumed to be located above the water table where the soil is unsaturated.

According to the assumptions mentioned above, the factor of safety (F.S.) for the 2D infinite slope (Fig. 16a) is determined by comparing the resisting shear force (T_f) along the slip surface with the driving force due to the weight ($W_{sin}\alpha$):

$$F.S. = \frac{T_f}{W sin\alpha} \tag{10}$$

where W is the weight of the element

The force normal to the failure surface is:

$$N = W cos\alpha = \gamma h l 1 \cos^2\alpha \tag{11}$$

The width of the element is assumed to be 1 m.

$$F.S. = \frac{\gamma h l cos^2\alpha \tan\varphi' + S_r s \tan\varphi' l + c_{r\_b} l}{\gamma h l \sin\alpha \cos\alpha} \tag{12}$$

$$F.S. = \frac{\tan\varphi'}{\tan\alpha} + \frac{2S_r s \tan\varphi'}{\gamma h \sin 2\alpha} + \frac{2c_{r\_b}}{\gamma h \sin 2\alpha} \tag{13}$$

where γ is the unit weight of the soil in-situ, the c_{r_b} is the root reinforcement at the base of the element and b, h, α are geometric parameters defining the element in the infinite slope (Fig. 16a).

The first term on the right hand side of the equation (13) is the contribution of friction angle, the second term is the effect of apparent cohesion due to the unsaturated conditions, and third part is the contribution of the base root reinforcement.

The reinforcing effect of the roots in this section is conceptualised as resistant shear and normal tensile stresses, along the sides and base, and the upper face of the failure wedge, respectively. Estimates of the root reinforcement mobilised for the Ruedlingen slope are based on the distribution of the roots and the mechanical properties of the root bundles as a function of the displacement during pull out tests [SCHWARZ, 2011].

Perpendicular root models are used in conventional methods of root reinforcement quantification [WALDRON, 1977; WU *et al.*, 1979; WU *et al.*, 1988; WU and WATSON, 1998]. In these models, it is assumed that the roots are located normal to shear zone and tension is transferred to them as the faces of the shear band are moving relative to each other. Confining stress increases due to the tensile force in the reinforcements [BUCHER, 1983]. Another important assumption of this method is that the full tensile strength of the roots is mobilised as the shear occurs (e.g. POLLEN and SIMON, 2005). However, field and laboratory measurements of Ruedlingen case show that the maximum root bundle strength occurs

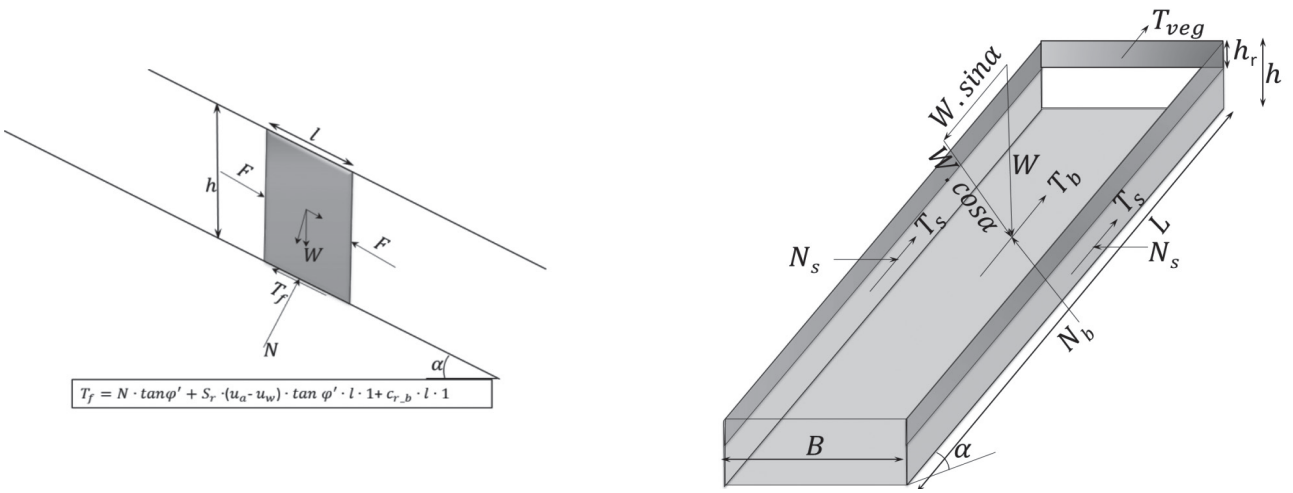

Fig. 16 – a) The infinite slope model; b) The simplified three dimensional model.
Fig. 16 – a) Modello di pendio indefinito; b) Modello tridimensionale semplificato.

at larger strains than the typical strains at the maximum soil strength.

This two dimensional limit equilibrium analysis (SPRINGMAN *et al.*, 2003; CASINI *et al.*, 2010b) is now extended to a three dimensional geometry with laterally limited slides, in order to account for the resisting forces along the sides (T_s) of the failure wedge (Fig. 16b). The vertical and lateral reinforcing effect of the vegetation at the base and along the vertical planes of the failure wedge is estimated, respectively. The effective depth of lateral root reinforcement (h_r) can be varied. Moreover, the effect of frictional resistance due to the horizontal soil pressures acting on the walls and the apparent cohesion are taken into account.

The factor of safety is again calculated by equation (10):

$$F.S. = \frac{T_f}{W\sin\alpha} = \frac{T_b + 2T_s}{W\sin\alpha} \qquad (14)$$

where, T_b and T_s are the resisting forces mobilised at the base and at the side of the block, respectively.

The resisting force at the base (T_b) is:

$$T_b = N_b \tan\varphi' + S_r\, s \tan\varphi'\, BL + c_{r\_b} BL \qquad (15)$$

where *B, L* are the width and the length of the block respectively, (Fig. 16b), and N_b is the normal force to the base plane:

$$N_b = W\cos\alpha = \gamma\, hBL\cos^2\alpha \qquad (16)$$

where, γ and h are the unit weight of the soil and the height of the wedge, respectively.

The resisting force at the sides of the wedge is:

$$T_s = N_s \tan\varphi' + S_r\, s \tan\varphi'\, hL + c_{r\_b}\, h_r\, L \qquad (17)$$

where c_{r_s} is the root reinforcement at the sides of the element, h_r is the height of the root reinforcement (Fig. 16b), and N_s is normal force applied to the sides. For the sake of simplicity, a constant value of suction along the depth of the soil to the failure surface is assumed in this equation.

$$N_s = \frac{1}{2} K\gamma'\, L h^2 \qquad (18)$$

According to Equations (14) to (18) and assuming a horizontal pressure coefficient at rest (K_0=*1-sin* φ'), the factor of safety will be:

$$F.S. = \frac{\gamma\, hBL\cos^2\alpha\, \tan\varphi' + S_r s \tan\varphi'\, BL + c_{r\_b} BL}{\gamma hBL\cos\alpha\, \sin\alpha} + \\ + \frac{2(1/2\, K_0 \gamma L h^2 \tan\varphi' + S_r s \tan\varphi' hL\cos\alpha + c_{r\_s} h_r L\cos\alpha)}{\gamma hBL\cos\alpha\, \sin\alpha} \qquad (19)$$

$$F.S. = \frac{S_r s \dfrac{\tan\varphi'}{\cos^2\alpha}\left[1 + \dfrac{2h}{B}\cos\alpha\right] + \gamma h \tan\varphi'\left[1 + \dfrac{K_0 h}{B\cos^2\alpha}\right] + \\ + \dfrac{\dfrac{c_{r\_b}}{\cos^2\alpha} + \dfrac{2h_r c_{r\_s}}{BL\cos\alpha}}{\gamma h \tan\alpha}}{\gamma h \tan\alpha} \qquad (20)$$

The forces acting at the upper and lower ends of the block are ignored in this method, except for the root reinforcement, T_{veg}, which is evaluated in section 7.3.

Parameters used for the soil, root reinforcement, and geometry in these analyses are listed in Table III.

Tab. III – Parameters used for the infinite slope analyses.
Tab. III – Parametri usati nell'analisi di pendio indefinito.

φ' (°)	γ (kN/m³)	e	α (°)	h (m)	L (m)	b (m)	c_{r_b} (kPa)	c_{r_s} (kPa)	h_r (m)
32	16.33	1	38	1.1	17	7.5	0.5	4	0.3

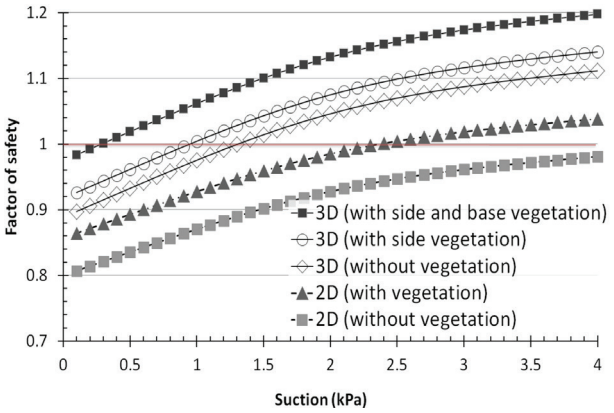

Fig. 17 – Comparison between 2D infinite slope and simplified 3D analysis, with and without vegetation.
Fig. 17 – Confronto tra le analisi di pendio indefinito 2D e 3D semplificata con e senza vegetazione.

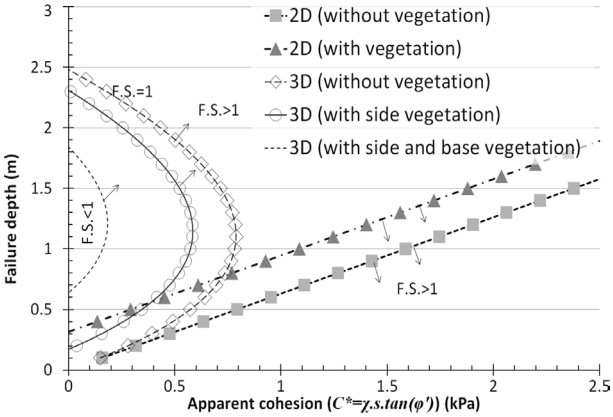

Fig. 18 – Minimum required apparent cohesion for different failure depths (the arrows show the regions with F.S.>1).
Fig. 18 – Coesione apparente minima necessaria per diverse profondità di rottura (le frecce indicano la regione con F.S.>1).

The comparison between the 2 approaches based on equations (13) and (20), with different assumptions for the root reinforcement, is illustrated in figure 17. The factor of safety is calculated based on the wetting branch of the water retention curve for Ruedlingen soil, with e = 1.0 (Fig. 10).

The results show that the F.S. derived from the 2D approach for suctions lower than 4 kPa is 88% of the F.S. of 3D approach for the failure width of 7.5 m (on average).

The value for the reinforcing effect of the lateral roots is based on an extensive study of the pull-out and breakage forces of roots in the region. The selected value (c_{r_s} = 4 kPa) is an average of the measured maximal root reinforcement at the scarp of the failure zone. The measured values of the lateral root reinforcement vary between 0 to more than 10 kPa on this slope [SCHWARZ, 2011].

The lateral root reinforcement is assumed to be uniformly effective at depths of 0 to 0.3 m in these analytical simulations. Comparing the changes in the F.S. shown in figure 17 for the 3D models, with and without lateral root reinforcement, it can be seen that the difference in the predicted F.S. is about 3%. This value shows the effect of cutting the roots along the longitudinal borders of the experiment site on the stability of this marginally stable slope.

6.2. Prediction of potential depth of failure surface

The F.S. is set to 1.0, to establish the variation of minimum required suction (or degree of saturation) with the depth of the inclined failure plane, in order to predict the potential depth of failure and hence the volume of mobilised material [CASINI *et al.*, 2010b]. This is a key factor in landslide hazard assessment.

Equations (21) and (22) show the minimum apparent cohesion required to have a stable slope, in the 2 and 3 dimensional cases, respectively.

$$F.S. = 1 \Rightarrow c^* = \left[1 - \frac{\tan\varphi'}{\tan\alpha} - \frac{2c_{r\_b}}{\gamma h \sin 2\alpha}\right] \frac{\gamma h \sin 2\alpha}{2} \quad (21)$$

$$F.S. = 1 \Rightarrow c^* = \left[\gamma h \tan\alpha - \gamma h \tan\varphi' \left(1 + \frac{K_0 h}{B\cos^2\alpha}\right) - \frac{c_{r\_b}}{\cos^2\alpha} - \frac{2\, h_r c_{r\_s}}{B\cos\alpha}\right] \frac{\cos^2\alpha}{\left[1 + \frac{2h}{B}\cos\alpha\right]} \quad (22)$$

The results are depicted in figure 18. The 2D infinite slope methods, with different root reinforcement at the base, show an increasing value of required apparent cohesion as the depth of failure increases. The 3D approach results in a critical depth of around 1.3 m as the suction decreases. This depth is similar in different scenarios of root reinforcement and agrees well with the average depth of failure in reality (h_{ave} = 1.1 m).

6.3. Effect of variability of root reinforcement with depth

The vertical distribution of tree roots in the soil profile along the scarp is confined to the top 0.6 m of soil, whereas the root network of the grass plants was only effective in the first 0.2 m of soil, as reported by SCHWARZ [2011]. The root network for both trees and grass plants decays exponentially with depth, similar to the findings of previous researchers (e.g. ABE and IWAMOTO, 1990; SCHMIDT *et al.*, 2001; DOCKER and HUBBLE, 2009). Accordingly, a conceptual model for the lateral root reinforcement is considered with an exponential decay in cohesion attributed to the roots from 0.15 m to 0.6 m in depth (Fig. 19a). The same

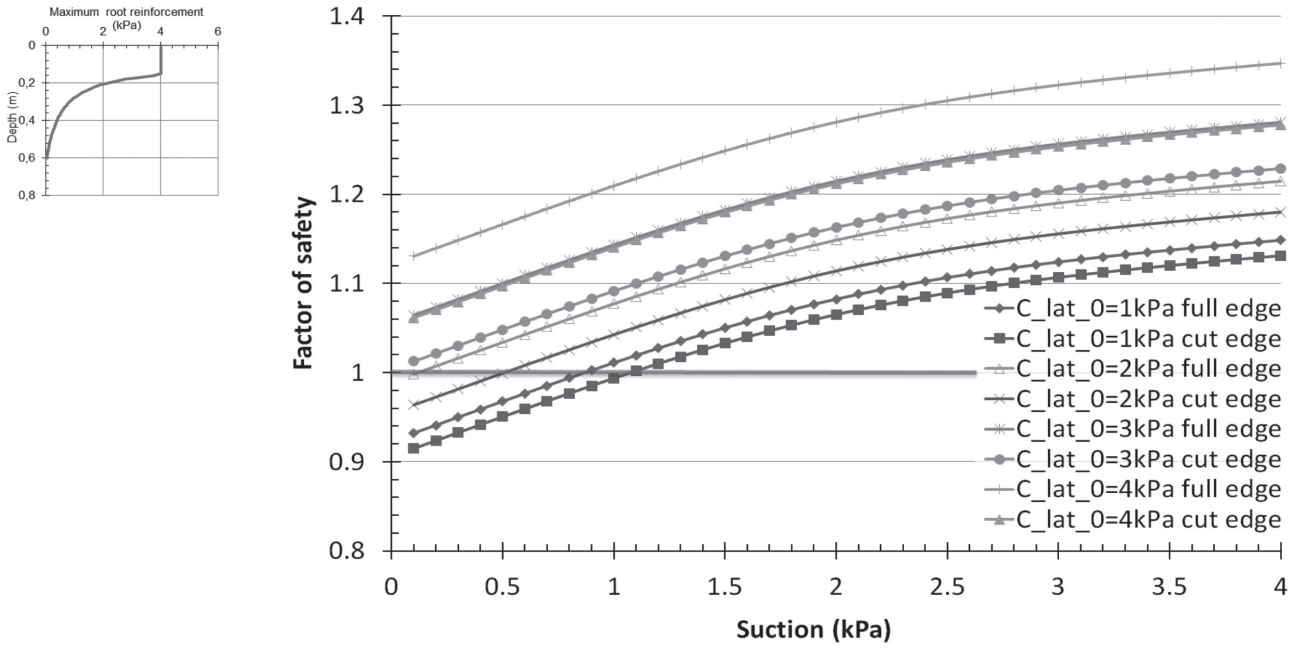

Fig. 19 – a) Conceptual model for decay of root reinforcement with depth; b) Parametric study on the stability effect of the maximum lateral root reinforcement.

Fig. 19 – a) Modello concettuale di decadimento del rinforzo delle radici con la profondità; b) Studio parametrico della stabilità dovuta al rinforzo laterale delle radici.

approach will be applied, as in section 6.1, to calculate the factor of safety, with the difference of variable root effects and application of root reinforcement to the both side and back of the failure wedge (T_{veg} in Fig. 16b). No basal root reinforcement is taken into account in this section.

Similar to equation (14), the F.S. can be written as:

$$F.S. = \frac{T_f}{W\sin\alpha} = \frac{T_b + 2T_s + T_{veg}}{W\sin\alpha} \qquad (23)$$

T_b is similar to equation (15) but without the term accounting for the base root reinforcement.
T_s is the shear resistance on one side of the failure wedge:

$$T_s = N_s \tan\varphi' + S_r\, s \tan\varphi'\, hL + F_{veg\_s} \qquad (24)$$

where N_s is the normal force applied to the sides and is calculated according to Equation (18), and F_{veg_s} is the reinforcing force of the vegetation on one side of the failure wedge:

$$F_{veg\_s} = \cos^2\alpha \int_0^{h_r} c_{lat} L\, dh \qquad (25)$$

where c_{lat} is the value of root reinforcement, according to Figure 19a.

Likewise, the reinforcing force provided by the vegetation at the back of the failure wedge (T_{veg}) (Fig. 16b) is:

$$T_{veg} = \int_0^{h_r} c_{lat} B\, dh \qquad (26)$$

The factor of safety is compared for the first and the second experiments, after cutting the roots along the longitudinal borders of the field. Figure 19b, shows the changes in the F.S. with respect to the decrease in suction and the changes in the maximum value of the root reinforcement. The effect of cutting the roots to the depth of 0.3 m along the longitudinal bounds of the slope on the F.S. is considered. c_{lat_0} is the cohesion attributed to the roots at the depth of 0 m of the soil. The difference in the F.S. between the first (full edge) and the second (cut edge) experiments is about 7% for the top root reinforcement of $c_{lat\_0} = 4$ *kPa*. However, the factor of safety is not lower than 1.0 within the positive range of matric suction (negative pore water pressure), if $c_{lat\_0} > 3$ *kPa*.

7. Two dimensional uncoupled numerical simulations

The results of the uncoupled numerical simulations of the first and the second experiments are presented in this section. The simulations were performed using the SEEP/W and SLOPE/W modules of the GeoStudio software. The hydraulic boundary conditions were applied to the finite element model produced with the SEEP/W and pore pressure distributions were calculated. The factor of safety

of the slope was determined using SLOPE/W and based on the pore pressure distributions exported from SEEP/W for each time step. The pore pressure distributions were calculated according to the Richards' equation [RICHARDS, 1931] for pore fluid flow in the unsaturated soil matrix. The laboratory results of water retention curve were fitted with the formula proposed by VAN GENUCHTEN [1980]. The unsaturated hydraulic conductivity functions derived by BECK [2010] were calibrated and used in the analysis.

The shear strength of the unsaturated soils was applied in SLOPE/W using FREDLUND *et al.* [1978] extended form of the Mohr-Coulomb criterion (Eq. 24).

$$\tau_f = c' + (\sigma' - u_a)\tan\varphi' + (u_a - u_w)\tan\varphi^b \qquad (27)$$

where φ^b describes the linear increase of the shear strength due to the increase of matric suction. This linear expression has been questioned in view of increasing experimental evidence [ESCARIO and SAEZ, 1986; FREDLUND *et al.*, 1987; ALONSO *et al.*, 1990]. Unfortunately, this cannot be considered by the GeoStudio software.

The relationship between φ' and φ^b can be derived by comparing equations 1 and 27.

$$\frac{\tan\varphi^b}{\tan\varphi'} = S_r = \frac{\theta}{n} \qquad (28)$$

The most conservative value for φ^b is used in these simulations based on the residual volumetric water content and maximum insitu porosity.

The mechanical properties used for these simulations are summarised in table IV.

The reinforcement effect of the roots is implemented in the mechanical properties of the model by introducing additional cohesion (c_{veg}) to the upper 0.3 m of the top soil layer. The value is chosen based on the average measurements in the field [SCHWARZ and RICKLI, 2008]. The calculation of the factor of safety is performed based on the method of slices and with the approach of MORGENSTERN and PRICE [1965], which considers the moment equilibrium of individual slices.

The geometry of the bedrock is derived from the DPL results. From the hydraulic point of view, the bedrock is impermeable. It is also assumed to be mechanically stable under the simulated loads. It is modelled as an elastic material. The location and sizes of the fissures in the bedrock were determined by monitoring the sequences of the changes in the degree of saturation in the soil and bedrock regions. The fissures were implemented in the geometry of the models and were *filled* with the overlying soil, with similar hydro-mechanical properties. This assumption needs to be refined by further field investigations or by a parametric study of the hydraulic properties of the fissures and their effect on the drainage of the slope.

Tab. IV – Mechanical properties adopted for the numerical simulations.
Tab. IV – Proprietà meccaniche usate nelle simulazioni numeriche.

γ (kN/m^3)	φ' (°)	φ^b (°)	c' (kN/m^2)	c_{veg} (kN/m^2)
16.3	32	10	0	4

7.1. Simulation of the monitoring experiment (October 2008)

Figure 20 shows the geometry of the bedrock, location of the fissures, water flow paths and the saturated zone in the slope at the last time step before the rainfall stopped in the first Ruedlingen experiment. Infiltrating water flows towards and is drained by means of the fissures in the bedrock. Accordingly, it is assumed that these permeable fissures play a major role in stabilising the slope. The calculated factor of safety is lower than 1, for the critical slip surface of the first experiment but this simulation is a 2 dimensional one, and does not take into account the side friction mobilised at the lateral boundaries of the failure wedge. Therefore, the simulated pore pressures were used in a simplified 3 dimensional limit equilibrium model, as explained in section 6.1. As a result, the F.S. increased to 1.13, which implies stability and is consistent with movements in the slope during the first experiment, but without developing failure.

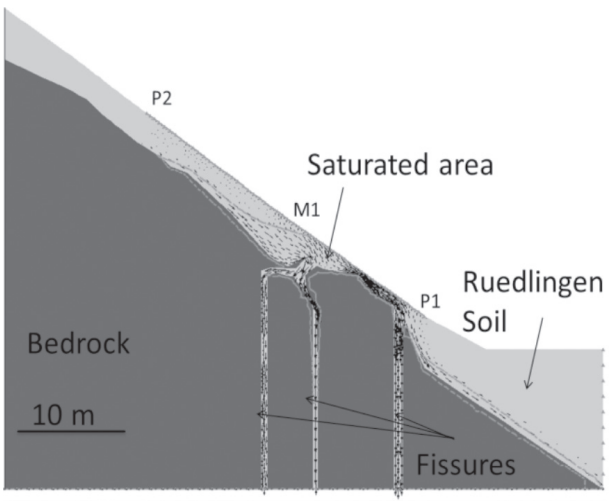

Fig. 20 – Water flow paths and the saturated zone at the end of the rainfall [BISCHOF, 2010].
Fig. 20 – Percorsi del flusso d'acqua e zona di completa saturazione al termine dell'evento di pioggia [BISCHOF, 2010].

7.2. Simulation of the triggering experiment (March 2009)

7.2.1. HYDRAULIC SIMULATIONS

The simulations were performed for the second experiment based on the geometry of the bedrock on the right hand side of the field (looking from the road) because the ERT measurements were performed on this side and also the failure occurred mainly on the right side of the slope. The ERT measurements and also field observations after the failure indicate a fissure and a permeable horizontal intrusion in the upper part of the bedrock (Fig. 20).

Since the rain intensity was not uniformly distributed on the slope in the second experiment [ASKARINEJAD *et al.*, 2010b], seven zones were defined over which different intensities were applied.

The infiltration simulations showed that the majority of the rain applied in the upper part of the slope was drained into the sub-vertical fissure and then through the horizontal intrusion to the slope body, applying an uplifting seepage force to the soil. This could be one of the main causes of triggering the failure. The inclination of the upper fissure was not clear either from the ERT measurements or from the field investigations. Therefore, a parametric study was performed on the effect of the inclination of this fissure. The results showed that a range of directions of fissures provide different time spans for the water to reach the interface between the bedrock and the soil through the permeable horizontal intrusion. Hence, the inclination can delay the exfiltration of water from the bedrock.

The suction changes were monitored in the upper part of the model corresponding to the location of cluster 3 (C.3 in Fig. 5) on the slope. One of the monitoring points on the model was on the surface, and the other one was at the interface between the soil and the bedrock, at a depth of 1.2 m. Figure 21 shows the comparison between the simulated suctions from the numerical model and the measured suction in-situ. The curves follow similar trends. The increase of suction at the surface due to ceasing application of rain can be seen in the data obtained from the numerical solution.

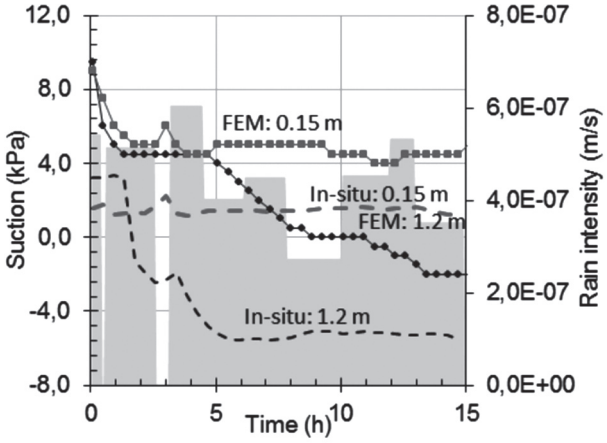

Fig. 21 – Comparison between the simulated suction changes to the in-situ measured values (after BISCHOF, 2010).
Fig. 21 – Confronto tra suzione misurata e ottenuta dalle simulazioni numeriche (da BISCHOF, 2010).

The difference of 2 to 3 kPa between the measured and simulated values of suction could have several causes, such as the uncertainties and simplifications in the model, the precision of the measurements, and the difference in the initial conditions of pore water pressure between the model and the slope in reality.

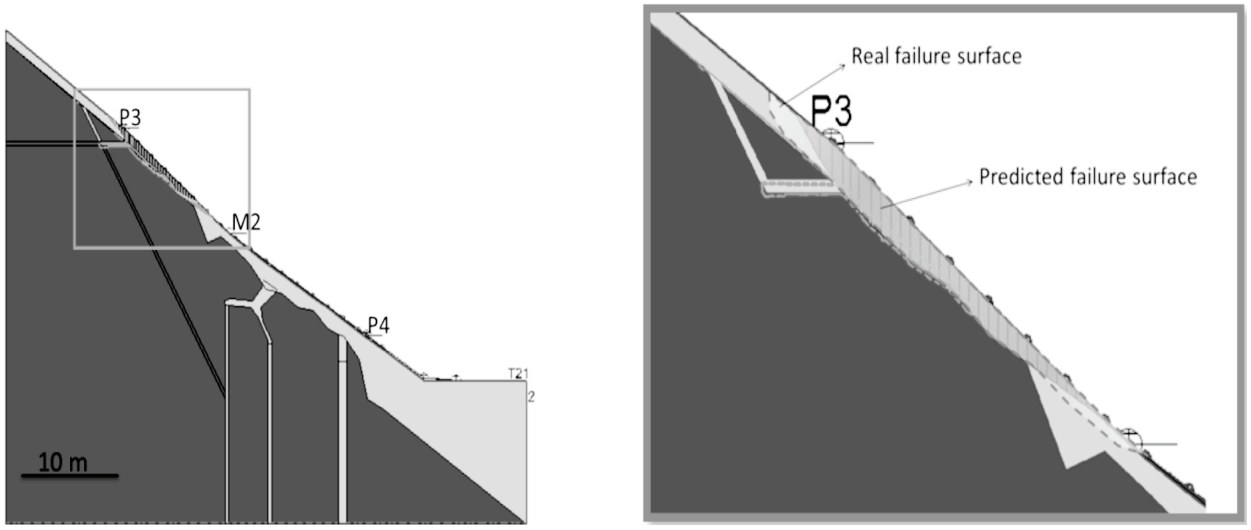

Fig. 22 – a) The geometry of the bedrock on the right hand side of the slope and location of the critical slip surface; b) Enlarged section showing the critical slip surface and the saturated zone (dashed curve) [BISCHOF, 2010].
Fig. 22 – a) Geometria del substrato roccioso a destra del pendio e posizione della superficie critica; b) Sezione ingrandita della superficie di scorrimento critica e zona di completa saturazione (zona tratteggiata), [BISCHOF, 2010].

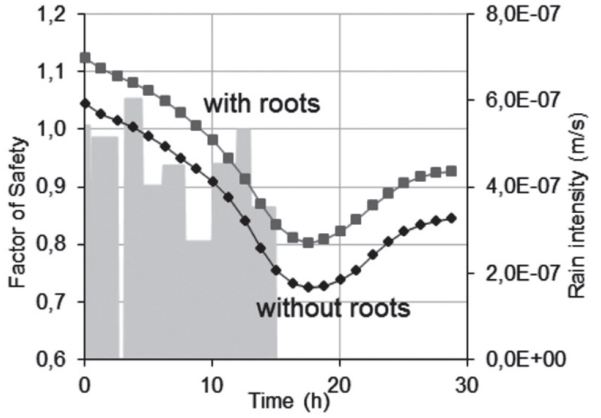

Fig. 23 – Comparison of the changes in F.S. for the slope with or without root reinforcement [BISCHOF, 2010].
Fig. 23 – Confronto dell'evoluzione del fattore di sicurezza per il pendio con e senza il contributo delle radici [BISCHOF, 2010].

7.2.2. FACTOR OF SAFETY

No reinforcing effects of the roots were taken into account in these simulations, because the roots along the sides of the slope were severed to the depths of 0.3 to 0.4 m before the experiment, although this is only relevant for the right hand boundary of the failure zone (Fig. 5).

The critical slip surface based on the method of slices, (which is quite similar to the real slip surface) has a factor of safety equal to 0.76, after 15 hours of rainfall. After performing the corrections for the 3 dimensional effects, and without root reinforcement, F.S. = 0.83.

The critical slip surface is shown in figure 22.

7.3. Root reinforcement effect in the second experiment

Analyses have been conducted with root reinforcement over the upper 0.3 m of the soil layer. The comparisons are shown in figure 23. The factor of safety increases with a magnitude of 0.1 during the experiment, after introducing the root effects. The minimum value of F.S. is reached 3 hours after the rainfall stops.

8. Summary and conclusions

Field and laboratory investigations have provided a comprehensive set of data both to characterise the ground and to record the hydro-mechanical responses of a silty sand slope during artificial rainfall events. The hydrological characterisations revealed a bottom to top saturation pattern [SPRINGMAN *et al.*, 2012] for the soil profile in the study area, and also the possibility of drainage into the bedrock.

A comprehensive laboratory characterisation has been performed on natural and statically compacted samples of Ruedlingen soils. Since the average slope of the field exceeds the critical state internal friction angle, the partial saturation and the reinforcement of the root and possibly the shape of the bedrock combine to play a fundamental role in stabilising the slope.

The instantaneous profile method was used to derive the hydraulic conductivity function of the soil in unsaturated conditions. The results [BECK, 2010] show a decrease of two orders of magnitude in the conductivity with increasing suction to 40 kPa.

The spatial distributions of reinforcing effects of the roots were studied. The reinforcement was quantified and used in the analytical and numerical simulations. However, the estimated values for the root reinforcement along the scarp of the failure were higher than the values that were back calculated from the limit equilibrium method. Apart from the simplifications made in the models, one reason for this difference can be that the fine roots have a strong seasonality; hence there are less superficial fine roots in winter (when the landslide occurred) than in summer (when the calibration was done) [SCHWARZ, 2011].

Photogrammetry was successfully used to monitor the surface movements during the slope monitoring and landslide triggering experiments and helped to identify the area of the slope most at risk prior to failure. This has important implication for early warning systems and counters the assumption that such failures are abrupt and lack early clues and limited possibility of forecasting [CAMPBELL 1975].

The mechanical features of unsaturated soils and reinforcing effects of the vegetation were implemented in simple infinite slope limit equilibrium analysis and results were compared to the analytical three dimensional limit equilibrium simulations. The three dimensional geometries included laterally limited slides of the failure wedge. Basal and lateral root reinforcements have been introduced in these models. The results show reasonable values for the factor of safety, despite the simplifications in these models.

Based on these simplified 3-D models, the possible depth of the failure surface was calculated at 1.1 m (Fig. 18) for a factor of safety of 1. The calculated values agreed quite well, with the in-situ measurements at 0.8 to 1.3 m.

As confirmed by the 2D uncoupled hydro-mechanical finite element simulations, the hydraulic interaction of the bedrock with the overlying soil layers, in terms of drainage and exfiltration, can play a major role in the pattern of pore pressure distributions and in stabilising or destabilising the slopes. A more complex 3D finite element analysis is being performed at present in order to take the coupled response of soils into account.

Acknowledgements

This research was partially funded by the Competence Centre for Environment and Sustainability (CCES) within the framework of the TRAMM – Project. Additional resources were provided by the ETH Research Fund and EU project SafeLand (EU FP7 grant agreement no. 226479). The authors are very grateful to the Ruedlingen Council, especially Mrs. Katy Leutenegger (President) and Martin Kern (Forest Manager), the fire station, the farmers, foresters and communities of Ruedlingen and Buchberg. Ernst Bleiker, Cornelia Brönnimann, Lorenzo Colombo, Matthias Denk, Sara Durot, Alfred Ehrbar, Francesca Gambazzi, Ralf Herzog, Gernot Michlmayr, Ferney Morales, Christian Rickli, Rene Rohr, Andreas Schmid, Massimiliano Schwarz, Marco Sperl, Manfred Staehli, Karl Steiner, Barbara Suski, Axel Volkwein, Albrecht Von Boetticher, Corinna Wendeler, Felix Wietlisbach and Adrian Zweidler are thanked for their many and varied contributions to this project.

The authors acknowledge the two anonymous reviewers for their detailed and helpful comments to the manuscript.

References

ABE K., IWAMOTO M. (1990) – *Simulation model for the distribution of tree roots application to a slope stability model.* Japanese Forestry Society, 72, pp. 375-387.

AKCA D., GRUEN A., ASKARINEJAD A., SPRINGMAN S.M. (2011) – *Photogrammetric monitoring of an artificially generated landslide.* International Conference on Geo-information for Disaster Management (Gi4DM), Antalya, Turkey, Published on CD-ROM only.

ALONSO E.E., GENS A., DELAHAYE C. (2003) – *Influence of rainfall on the deformation and stability of a slope in overconsolidated clays: a case study.* Hydrogeology Journal, 11, n. 1, pp. 174-192.

ALONSO E.E., GENS A., JOSA A. (1990) – *A constitutive model for partially saturated soils.* Géotechnique, 40, n. 3, pp. 405-430.

ASKARINEJAD A. (2009) – *A method to locate the slip surface and measuring subsurface deformations in slopes.* 4th International Young Geotechnical Engineers' Conference, Alexandria, Egypt, pp. 171-174.

ASKARINEJAD A., CASINI F., KIENZLER P., SPRINGMAN S.M. (2010a) – *Comparison of the in situ and laboratory water retention curves for a silty sand.* 5th Intern. Conf. Unsaturated Soils UNSAT, Barcelona, Spain, pp. 423-428.

ASKARINEJAD A., CASINI F., KIENZLER P., TEYSSEIRE P., SPRINGMAN S.M. (2010b) – *Mountain risks: two case histories of landslides induced by artificial rainfall on steep slopes.* International Conference of 'Mountain Risks: Bringing Science to Society', Florence, Italy, pp. 201-206.

BECK A. (2010) – *Measurement of unsaturated hydraulic conductivity with the instantaneous profile method.* Institute for Geotechnical Engineering, Zurich, Swiss Federal Institute of Technology, Semester project.

BISCHOF P. (2010) – *Modelling the interaction of the bedrock and slope in terms of drainage and exfiltration.* Institute for Geotechnical Engineering, Zurich, Swiss Federal Institute of Technology, Semester project.

BISHOP A.W. (1959) – *The principle of effective stress.* Teknisk Ukeblad, 106, n. 39, pp. 859-863.

BRÖNNIMANN C., TACHER L., ASKARINEJAD A., KIENZLER P., SPRINGMAN S.M. (2009) – *Pore water pressure modelling in a rainfall triggered shallow landslide: the sprinkling experiment in Rüdlingen, Canton Schaffhausen.* 7th Swiss Geoscience Meeting, Neuchâtel, Switzerland.

BUCHER F. (1983) – *Verfestigung von Böden durch Fasern.* Mitteilung der Schweizerischen Gesellschaft für Boden – und Felsmechanik (Pub. 108), pp. 65-68.

CAMPBELL R.H. (1975) – *Soil slips, debris flow and rainstorms in the Santa Monica Mountains and Vicinity, Southern California.* U.S. Geological Survey Professional Paper 851.

CASINI F., JOMMI C., SPRINGMAN S.M. (2010a) – *A laboratory investigation on an undisturbed silty sand from a slope prone to landsliding.* Granular Matter, 12, n. 3, pp. 303-316.

CASINI F., MINDER P., SPRINGMAN S.M. (2010b) – *Shear Strength of an unsaturated silty sand.* 5th International Conference of Unsaturated Soils, Barcelona, Spain, pp. 211-216.

COLOMBO L. (2009) – *Large shear box for analysing strength mobilisation in unsaturated conditions.* Milano, Politecnico di Milano Master thesis.

DOCKER B.B., HUBBLE T.C.T. (2009) – *Modelling the distribution of enhanced soil shear strength beneath riparian trees of south-eastern Australia.* Ecological Engineering, 35, pp. 921-934.

ESCARIO V., SAEZ J. (1986) – *The shear strength of partly saturated soils.* Géotechnique, 36, n. 13, pp. 453-456.

FISCHER C., LÓPEZ J., SPRINGMAN S.M. (2003) – *Remediation of an eroded steep slope in weathered sandstone after a major rainstorm.* International Conference on Landslides. Hong Kong, pp. 878-883.

FREDLUND D.G., MORGENSTERN N.R., WIDGER R.A. (1978) – *The shear strength of unsaturated soils.* Canadian Geotechnical Journal, 15, n. 3, pp. 313-321.

FREDLUND D.G., RAHARDJO H., GAN J.K.M. (1987) – *Nonlinearity of strength envelope for unsaturated soils.* 6th Int. Conf Expansive Soils, New Delhi, pp. 49-54.

GAMBAZZI F., SUSKI B. (2009) – *Electrical Resistivity Tomography Rüdlingen.* Internernal Tramm meeting, ETH Zurich, Switzerland.

HAN C., VARDOULAKIS I. (1991) – *Plane-strain compres-*

sion experiments on water-saturated finr-grained sand. Géotechnique, 41, n. 1, pp. 49-78.

HARP E.L., WELLS W.G., SARMIENTO J. (1990) – *Pore pressure response during failure in soils.* Geological Society of America Bulletin, 102, pp. 428-438.

HEAD K.H. (1998) – *Manual of soil laboratory testing, 3.* Effective stress tests Wiley, Chichester.

KIENZLER P. (2007) – *Experimental study of subsurface stormflow formation.* Diss-Nr. 17330 Hydrology, Zurich, ETH Zurich.

KIENZLER P. (2008) – *The Ruedlingen experiment; hydrologycal chaeacterisation.* Internernal Tramm meeting, Zurich.

LEHMANN P., GAMBAZZI F., SUSKI B., BARON L., ASKARINEJAD A., SPRINGMAN S.M., HOLLIGER K., OR D. (2012) – *Evolution of wetting patterns preceding hydro-mechanically induced landslide inferred from electrical resistivity tomography.* Water Resources Research (under review).

MORGENSTERN N.R., PRICE V.E. (1965) – *The Analysis of the Stability of General Slip Surfaces.* Géotechnique, 15, pp. 79-93.

NG C.W.W., SHI Q. (1998) – *Influence of rainfall intensity and duration on slope stability in unsaturated soils.* Quarterly Journal of Engineering Geology, 31, pp. 105-113.

NOCILLA A., COOP M.R., COLLESELLI F. (2006) – *The mechanics of an Italian silt: an example of 'transitional' behaviour.* Géotechnique, 56, n. 4, pp. 261-271.

OCHIAI H., OKADA Y., FURUYA G., OKURA Y., MATSUI T., SAMMORI T., TERAJIMA T., SASSA K. (2004) – *A fluidized landslide on a natural slope by artificial rainfall.* Landslides, 1, pp. 211-220.

OKA H. (1972) – *Impacts by the "artificial landslide": reexamine the rage of nature* [in Japanese]. Kagaku Asahi, 32, n. 1, pp. 152-153.

OOSTERBAAN R.J., NIJLAND H.J. (1994) – *Determining the saturated hydraulic conductivity.* Drainage Principles and Applications, International Institute for Land Reclamation and Improvement (ILRI) Publication 16. H.P. Ritzema, Wageningen, The Netherlands, pp. 435-476.

POLLEN N., SIMON A. (2005) – *Estimating the mechanical effects of riparian vegetation on stream bank stability using a fiber bundle model.* Water Resources Research, 41, W07025,http://dx.doi.org/07010.01029/02004WR003801.

RICHARDS L.A. (1931) – *Capillary conduction of liquids through porous medium.* Physics, 1, pp. 318-333.

SCHMIDT K.M., ROERING J.J., STOCK J.D., DIETRICH W.E., MONTGOMERY D.R., T.S. (2001) – *The variability of root cohesion as an infuence on shallow landslide susceptibility in the Oregon Coast Range.* Canadian Geotechnology Journal, 38, pp. 995-1024.

SCHWARZ M. (2011) – *Hydro-mechanical characterization of rooted hill slope failure: from field investigations to fibre bundle modelling.* ETH Zurich, PhD.

SCHWARZ M., RICKLI C. [2008] *Characterisation of the vegetation cover at the test site of Ruedlingen.* Internal GEOLEP CCES-TRAMM report.

SIEBER R. (2003) – *Atlas der Schweiz–interaktiv: karten zur Bevölkerungsentwicklung.* Bundesamt für Landestopographie,Wabern.

SPRINGMAN S.M., ASKARINEJAD A., CASINI F., FRIEDLE S., KIENZLER P., TEYSSEIRE P., THIELEN A. (2012) – *Lessons learnt from field investigations in potentially unstable slopes in Switzerland.* Slovenian Geotechnical Journal (In print).

SPRINGMAN S.M., JOMMI C., TEYSSEIRE P. (2003) – *Instabilities on moraine slopes induced by loss of suction: a case history.* Géotechnique, 53, n. 1, pp. 3-10.

Springman S.M., Kienzler P., Casini F., Askarinejad A., (2009) – *Landslide triggering experiment in a steep forested slope in Switzerland.* 17th International Conference of Soil Mechanics and Geotechnical Engineering, Alexandria, Egypt, pp. 1698-1701.

TACHER L., LOCHER D. (2008) – *Geological Characterization of the Buchberg field site (Ruedlingen).* Internal TRAMM Report.

TERZAGHI K. (1936) – *The shear resistance of saturated soils and the angle between the planes of shear.* 1st International Conference on Soil Mechanics, pp. 54-56

TEYSSEIRE P. (2005) – *Geotechnische Eigenschaften von Moränen, Diss-Nr. 16322.* Institute for Geotechnical Engineering Zürich, ETH Zürich.

VAN GENUCHTEN M.T. (1980) – *A closed-form equation for predicting the hydraulic conductivity of unsaturated soils.* Soil Sci. Soc. Am. J., 44, pp. 892-898.

WALDRON L.J. (1977) – *The shear resistance of root permeated homogeneous and stratified soil.* Soil Science Society of America Journal, 41, pp. 843-849.

WEILER M., NAEF F. (2003) – *An experimental tracer study of the role of macropores in infiltration in grassland soils.* Hydrological Processes 17: 477-493.

WU T.H., MCKINNEL W.P., SWANSTON D.N. (1979) – *Strength of tree roots and landslides on Prince of Wales Island, Alaska.* Canadian Geotechnical Journal, 16, pp. 19-33.

WU T.H., MCOMBER R.M., ERB R.T., BEAL P.E. (1988) – *Study of Soil-Root Interaction.* Journal of Geotechnical Engineering, ASCE, 114, pp. 1351-1375.

WU T.H., WATSON A. (1998) – *In situ shear tests of soil blocks with roots.* Canadian Geotechnical Journal, 35, n. 4, pp. 579-590.

YAGI N., YATABE R., ENOKI A. (1985) – *Laboratory and field experiments on prediction method of occurring time of slope failure due to rainfall* [in Japanese]. Landslide (Japanese Landslide Society), 22, n. 2, pp. 1-7.

YAMAGUCHI I., NISHIO K., KAWABE H., SHIBANO H., IIDA C. (1989) – *Initiation and fluidization of an artificial landslide: field experiment in Yui, Shizuoka Prefecture, Japan* [in Japanese]. Shinrin Kosoku (Areal Survey), 158, pp. 3-9.

Frane indotte da pioggia: un esperimento in sito su un pendio di sabbia con limo nel nord della Svizzera

Sono stati progettati ed eseguiti due esperimenti in scala reale su un pendio ripido con vegetazione situato a Ruedlinegn nel nord della svizzera, ad est del fiume Reno, nel cantone Sciaffusa. Fine degli esperimenti era quello di studiare i meccanismi di innesco delle frane superficiali indotte da pioggia. È stata effettuata un'estesa campagna sperimentale in sito, comprendente prove di caratterizzazione geotecnica, idrologica, delle radici, di mappatura idrogeologica e geofisica. Sono state eseguite prove in laboratorio in condizione di parziale e completa saturazione su provini naturali e ricostituiti, prelevati a diverse profondità nell'area prossima a quella di studio. Il sito è stato strumentato con strumenti tradizionali e innovativi. Sono state monitorate le seguenti grandezze: la pressione dell'acqua, il contenuto volumetrico d'acqua, la pressione totale, le emissioni acustiche, gli spostamenti superficiali e la profondità, la temperatura nel terreno e le grandezze meteorologiche. In questo lavoro le diverse grandezze misurate sono analizzate e confrontate per spiegare il comportamento di un pendio marginalmente stabile prima e durante la rottura indotta da pioggia. La stabilità del pendio è stata valutata utilizzando semplici metodi analitici e di analisi numerica che danno previsioni realistiche di un pendio prossimo alla rottura indotta da aumento della pressione dell'acqua. Il rinforzo laterale e alla base del pendio, dovuto alla vegetazione, e la parziale saturazione sono presi in considerazione nelle simulazioni bidimensionali e tridimensionali.